ANKARA YILDIRIM BEYAZIT UNIVERSITY
GRADUATE SCHOOL OF NATURAL AND APPLIED SCIENCES

ON THE DRAG OF A WARHEAD FRAGMENT FLYING AT DIFFERENT ORIENTATION ANGLES

M.Sc. Thesis by

Mahi Bilge BİLGİN

Department of Aerospace Engineering

November, 2024

ANKARA

ON THE DRAG OF A WARHEAD FRAGMENT FLYING AT DIFFERENT ORIENTATION ANGLES

A Thesis Submitted to the

Graduate School of Natural and Applied Sciences of

Ankara Yıldırım Beyazıt University

In Partial Fulfillment of the Requirements for the Degree of Master of Science in Aerospace Engineering, Department of Aerospace Engineering

by

Mahi Bilge BİLGİN

November, 2024

ANKARA

M.Sc. THESIS EXAMINATION RESULT FORM

We have read the thesis entitled "**ON THE DRAG OF A WARHEAD FRAGMENT FLYING AT DIFFERENT ORIENTATION ANGLES**" completed by **MAHİ Bilge BİLGİN** under supervision of **Assoc. Prof Dr. Mustafa KAYA** and we certify that in our opinion it is fully adequate, in scope and in quality, as a thesis for the degree of Master of Science.

Assoc.Prof.Dr. Mustafa KAYA

Supervisor

Dr. Mehmet MOLLAMAHMUTOĞLU

Jury Member

Dr. Muhammed ELMNEFİ

Jury Member

Prof. Dr. Sadettin ORHAN

Director

Graduate School of Natural and Applied Sciences

ETHICAL DECLARATION

I hereby declare that, in this thesis which has been prepared in accordance with the Thesis Writing Manual of the Graduate School of Natural and Applied Sciences,

- All data, information, and documents are obtained in the framework of academic and ethical rules,
- All information, documents, and assessments are presented in accordance with scientific ethics and morals,
- All the materials that have been utilized are fully cited and referenced,
- No change has been made to the utilized materials,
- All the works presented are original,

and in any contrary case of the above statements, I accept to renounce all my legal rights.

Date: 2024, 18 November **Signature:** _____

Name & Surname: Mahi Bilge BİLGİN

ACKNOWLEDGEMENTS

I would like to extend my heartfelt thanks to my advisor, Assoc. Prof. Dr. Mustafa KAYA, for their guidance and support throughout this research. I am grateful for the opportunity to learn from their experience and knowledge.

Beside my advisor, I would also like to extend my heartfelt thanks to Asst. Prof. Dr. Hürrem AKBIYIK, and Ress. Asst. Beyza Betül TANRIKULU for their invaluable support, guidance, and friendship. I extend my sincere gratitude to Remzi Can YILMAZ for his unwavering support and the motivation he provided throughout my work. Your encouragement and insights have greatly contributed to this work's success, and I deeply appreciate all that you have done. I would like to express my heartfelt gratitude to Şeyda ÖZTÜRK KİRİŞLİ for her unwavering friendship and support throughout our educational journey, as well as for contributing to our mutual growth." I would like to express my deepest gratitude to my beloved family for their support and motivation throughout my academic career. I am grateful for my mother, Zuhal, and father, Nazmi, for their love, and faith in me. To my dear sister Yıldız BİLGİN, your companionship and understanding have been invaluable. A special thank you to my brother Ress. Asst. Mehmet BİLGİN for his significant contributions to the writing of this thesis. Your support and assistance have been crucial in bringing this work to completion. I am forever grateful to have you all in my life.

November, 2024 **Mahi Bilge BİLGİN**

ON THE DRAG OF A WARHEAD FRAGMENT FLYING AT DIFFERENT ORIENTATION ANGLES

ABSTRACT

This study investigates the aerodynamic characteristics of a non-spherical fragment at Mach numbers 0.8, 1.0, and 1.2 across 30 distinct orientations, focusing on the drag coefficient (C_D) and drag force in each configuration. Results reveal significant variability in C_D values due to changes in orientation and exposed area, with values ranging widely at each Mach number.

In contrast, an average geometry derived from averaged coordinates consistently displayed lower C_D values and reduced drag forces, underscoring the potential of optimized configurations to achieve meaningful reductions in aerodynamic drag. The analysis also shows that while larger exposed areas generally lead to higher C_D values, this relationship is not strictly linear, indicating that shape and orientation play critical roles in aerodynamic behaviour.

In practical applications, using an average C_D for trajectory calculations provides a balance between computational efficiency and predictive reliability. This approach simplifies calculations and is particularly advantageous for real-time assessments, where computationally intensive orientation-specific models are less feasible. These findings highlight the importance of adaptable modelling techniques, such as machine learning-based surrogates, which can provide accurate aerodynamic predictions while minimizing computational demands. This study contributes to a better understanding of fragment dynamics in supersonic conditions and supports the development of efficient predictive models for safety-critical applications.

Keywords: Fragment, irregular shape, supersonic flow, drag coefficient

FARKLI YÖNELME AÇILARINDA UÇAN BİR HARP BAŞLIĞI PARÇACIĞININ SÜRÜKLENMESİ

ÖZ

Bu çalışma, 30 farklı yönelimde Mach sayıları 0.8, 1.0 ve 1.2'de küresel olmayan bir parçanın aerodinamik özelliklerini inceler ve her konfigürasyondaki sürükleme katsayısına (C_D) ve sürükleme kuvvetine odaklanır. Sonuçlar, yönelimdeki ve maruz kalan alandaki değişiklikler nedeniyle C_D değerlerinde önemli değişkenlik olduğunu ve değerlerin her Mach sayısında büyük ölçüde değiştiğini ortaya koymaktadır.

Buna karşılık, ortalama koordinatlardan türetilen ortalama geometrisi alınmış bir şekil, tutarlı bir şekilde daha düşük C_D değerleri ve azaltılmış sürükleme kuvvetleri gösterdi ve bu da ortalama geometrinin edilmiş konfigürasyonların aerodinamik sürüklemede anlamlı azalmalar elde etme potansiyelini vurguladı. Analiz ayrıca, daha büyük maruz kalan alanların genellikle daha yüksek C_D değerlerine yol açmasına rağmen, bu ilişkinin kesinlikle doğrusal olmadığını, şekil ve yönelimin aerodinamik davranışta kritik roller oynadığını göstermektedir.

Pratik uygulamalarda, yörünge hesaplamaları için ortalama bir C_D kullanmak, hesaplama verimliliği ve tahmin güvenilirliği arasında bir denge sağlar. Bu yaklaşım hesaplamaları basitleştirir ve özellikle hesaplama açısından yoğun yönelime özgü modellerin daha az uygulanabilir olduğu gerçek zamanlı değerlendirmeler için avantajlıdır. Bu bulgular, hesaplama taleplerini en aza indirirken doğru aerodinamik tahminler sağlayabilen makine öğrenimi tabanlı vekiller gibi uyarlanabilir modelleme tekniklerinin önemini vurgulamaktadır. Bu çalışma, süpersonik koşullarda parça dinamiklerinin daha iyi anlaşılmasına katkıda bulunmakta ve güvenlik açısından kritik uygulamalar için verimli tahmin modellerinin geliştirilmesini desteklemektedir.

Anahtar kelimeler: Parça, düzensiz şekil,süpersonik akış, sürükleme katsayısı

CONTENTS

NOMENCLATURE

List of Symbols

ν	Fluid Viscosity
ρ	Fluid Density
C_L	Lift Coefficient
C_D	Drag Coefficient
D	Drag Force
E	Energy
g	Gravitational Acceleration
Ma	Mach Number
Pr	Prandtl Number
Re	Reynolds Number
V	Velocity

Acronyms

ANN	Artificial Neural Network
CFD	Computational Fluid Dynamics
CFL	Courant–Friedricks-Levy
FCD	Flow Control Device
FGMR	Flexible Generalized Minimum Residual
JST	Jameson-Schmidt-Turkel
ML	Machine Learning
RANS	Reynolds-Averaged Navier-Stokes
SA	Spalart-Allmaras
SU2	Stanford University Unstructured
SWBLIs	Shock Wave-Laminar Boundary Layer Interactions
VBP	Volcanic Ballistic Projectiles

LIST OF TABLES

LIST OF FIGURES

CHAPTER 1

INTRODUCTION

In the last decades, the area of Computational Fluid Dynamics (CFD) has developed to such an extent that it is now an everyday tool for predicting and simulating the behavior of objects under most kinds of aerodynamic forces in a variety of fluid environments. Extensive utilization of CFD has been carried out in aerospace engineering to model how all kinds of objects—from the simplest geometries, like spheres, to non-spherical fragments—display their behavior under different flow regimes. These flow regimes range from subsonic and transonic to supersonic conditions; each condition presents unique challenges and requires different approaches in simulation. CFD simulations provide detailed insight into key aerodynamic forces like drag, lift, and pressure distributions, which are essential for understanding how particles move through the air. This capability to model fluid flow around objects with accuracy makes CFD a critical component in the design, analysis, and optimization of aerospace systems.

This great capability of CFD, from very low subsonic velocities to hypersonic flow regimes, makes it exceptionally useful in studying high-speed objects typical of debris or shrapnel fragments—highly irregular shapes that result in complicated and unforeseeable aerodynamic behavior. While analytical models may be sufficient to predict aerodynamic forces at lower speeds, as the Mach number increases into supersonic ranges, fluid dynamics become significantly more complex. Supersonic flow is marked by characteristics like shock waves, flow separation, and high turbulence, all of which can profoundly affect the aerodynamic forces at play. In such cases, the predictive power of CFD becomes crucial for accurately modeling these effects [1] [2].

One of the big advantages of CFD is its flexibility. It allows engineers to run flow simulations over both regular and irregular geometries under various flow conditions. This flexibility extends to a wide range of civil and defense aerospace applications, including missile fragment analysis, spacecraft re-entry debris, and aerodynamics for

novel aircraft configurations. For example, CFD simulations are commonly used to model the re-entry aerodynamics of blunt bodies, like spacecraft, and more streamlined designs, such as supersonic aircraft. [3] also highlighted the importance of CFD in analyzing space debris during re-entry, where shock-shock interactions and rarefied flows significantly influence the aerodynamic forces acting on fragments as they descend through different atmospheric layers.

When an object flies at supersonic speeds, it encounters a phenomenon known as shock wave formation. The shock waves are generated when the object's velocity exceeds the speed of sound, causing a sudden change in the pressure, temperature, and velocity of the surrounding air. These shocks introduce non-linearities into the fluid dynamics equations, making it much more difficult to accurately predict the aerodynamic forces on the object. For regular objects like spheres or cylinders, these shock interactions are well-understood and can be predicted fairly well [4]. However, for irregularly shaped objects like fragments, the constantly changing geometry as they tumble through the air makes shock wave interactions highly unpredictable. This adds a layer of complexity that CFD is uniquely suited to handle.

Aerodynamic drag, being one of the major forces opposing an object's motion through a fluid, is highly sensitive to the shape, orientation, and velocity of the object relative to the surrounding flow. While the drag coefficients for simple shapes like spheres are well-documented across various Mach numbers, for irregular shapes, these coefficients can vary greatly depending on the object's orientation relative to the flow. This variability in drag coefficient becomes especially critical for objects moving at supersonic speeds, where even slight changes in orientation or geometry can result in significant fluctuations in the aerodynamic forces acting on the object. Studies have shown that even minor differences in shape can lead to substantial variations in the drag coefficient, highlighting the importance of accurate modeling [5].

Beyond the forces of aerodynamics themselves, CFD is a crucial tool for design optimization. By accurately predicting the behavior of objects in supersonic flows, engineers can refine designs to enhance performance and reduce risks associated with high-speed flight or impacts. In the design of supersonic aircraft or missile systems,

CFD simulations help identify shapes that minimize drag and improve stability at high speeds. Similarly, in the defense industry, CFD is used to model the behavior of shrapnel and debris, providing key information for protective systems aimed at mitigating explosion effects. These surrogate models, based on CFD data, are increasingly used to predict aerodynamic forces for novel designs or conditions not yet fully explored, especially when combined with advanced techniques like machine learning.

The recent integration of machine learning techniques with CFD has opened new avenues for fast, data-driven predictions of aerodynamic forces. This is particularly valuable in cases where large-scale CFD simulations are prohibitively expensive for every scenario(Analysis of flow around. . .). Artificial Neural Networks, a subset of ML, have shown promise in learning from extensive CFD datasets to predict aerodynamic forces like drag, lift, and pressure distributions with high accuracy. Once trained, these ANN-based models can provide near-instant predictions for new shapes and configurations without the need for additional CFD simulations, saving significant time and computational resources [6].

In the field of supersonic particle analysis, ANNs provide a robust solution for handling the complexity of predicting aerodynamic behavior across various orientations and flow conditions. As [6] noted, irregularly shaped particles like shrapnel experience widely variable aerodynamic forces based on their orientation, making traditional empirical models unsuitable for accurate predictions. Surrogate models, trained on CFD-generated data, offer a more efficient and flexible approach to predicting drag coefficients across different flow regimes. These models are particularly valuable in aerospace applications where time-sensitive decisions must be made based on precise predictions of aerodynamic forces.

While the challenge of supersonic flow remains beyond traditional modeling techniques, CFD continues to be a vital tool for engineers seeking to understand and optimize the aerodynamic performance of objects in high-speed flight. The ability to realistically simulate and predict forces acting on irregular objects, such as shrapnel or debris, leads to improved designs and safer aerospace systems. By integrating CFD with emerging

technologies like machine learning, engineers can streamline the design process and push the boundaries of aerospace engineering. These advancements pave the way for future research into supersonic fragment behavior and offer new opportunities to enhance safety, performance, and reliability in the aerospace industry.

1.1 Challenges of Predicting Trajectories of Supersonic Fragments

Simulating the flight trajectories of supersonic fragments is a critical challenge, as high-speed aerodynamic interactions are complex, and the shapes of the fragments are often irregular. These challenges become more pronounced when dealing with fragments generated by high-velocity collisions, explosions, or aerospace debris, which typically exhibit unpredictable and chaotic flight patterns. The irregular geometries of such fragments introduce various nonlinear aerodynamic forces, making accurate modeling highly complex [7] [8]. One of the most significant challenges is determining the drag coefficient, which is crucial for predicting the trajectory of any object moving through a fluid. While the drag coefficient for regular, smooth objects like spheres or cylinders has been extensively studied, irregular fragments show great variability in their drag coefficients based on their shape, orientation, and exposed surface area [7] [5]. The tumbling motion of these irregular shapes makes the drag force dependent on specific conditions, making it difficult to develop generalized models [9] [10]. Research has also shown that even slight changes in a fragment's orientation can cause significant changes in the drag force, particularly in supersonic flow regimes where interactions with shock waves further complicate the flow field [11].

A key complicating factor at supersonic speeds involves shock wave interactions. When a fragment moves faster than the speed of sound, it generates shock waves that cause abrupt changes in pressure, temperature, and air density [12]. These shock waves introduce highly non-linear aerodynamic behavior, making it difficult to predict the forces acting on the fragment. While regular geometries can be modeled with reasonable accuracy, irregular shapes complicate the interactions between the fragment and the surrounding shock waves. Studies have shown that irregular fragments often experience significantly different aerodynamic forces depending on

their shape and orientation relative to the flow, leading to large variations in drag coefficients.

Boundary layer separation and wake formation further complicate the prediction of supersonic fragment trajectories. Boundary layer separation occurs when airflow detaches from the surface of the fragment, creating low-pressure areas behind it, which increase drag and affect the fragment's stability in flight [13] [12]. The turbulent wake behind a fragment traveling at supersonic speeds also complicates aerodynamic force predictions, as the wake's size and intensity vary based on the fragment's shape and speed. These phenomena are particularly challenging to predict for irregular fragments, as their tumbling motion presents different surface areas to the flow at any given time [14].

Another important challenge is the aerodynamic stability of supersonic fragments. The stability of a fragment in flight largely depends on the relative position of its center of pressure (CP) and center of mass (CM) [21]. If the CP is located too far forward from the CM, the fragment may become aerodynamically unstable, leading to uncontrollable tumbling and unpredictable trajectory changes. While the CP and CM of regular objects like projectiles can be calculated relatively easily, for irregular fragments, these properties depend heavily on the fragment's orientation. As a result, predicting the stability of an irregular fragment in supersonic flow is a complex task that requires a detailed analysis of its shape and aerodynamic characteristics.

This aerodynamic instability not only complicates trajectory predictions but also challenges the accurate measurement of drag coefficients. Measuring drag coefficients for irregular fragments adds further challenges [2]. Traditional methods such as wind tunnel tests and ballistic range experiments are impractical for many irregular shapes, especially at supersonic speeds. These fragments are difficult to test in controlled environments due to their unpredictable motion and varying surface areas exposed to the flow. Additionally, the equipment needed to simulate supersonic conditions for irregular fragments is expensive and difficult to calibrate, making it hard to collect accurate data for trajectory predictions.

In response to these challenges, Computational Fluid Dynamics (CFD) has become an important tool for analyzing the aerodynamics of supersonic fragments. CFD models the complex interactions between irregular fragments and the surrounding fluid, accounting for non-linear effects such as shock waves, boundary layer separation, and turbulent wake formation. By solving the Reynolds-Averaged Navier-Stokes (RANS) equations, CFD can provide detailed insights into the aerodynamic forces acting on irregular fragments at supersonic speeds. However, CFD is computationally expensive and time-consuming, particularly when modeling a wide range of orientations and flow conditions.

Recent advances in machine learning (ML) offer new opportunities to address these challenges. Surrogate models based on artificial neural networks (ANNs) can be trained on large CFD-generated datasets to predict drag coefficients and aerodynamic forces of irregular fragments under various conditions. Once trained, these models can make real-time predictions without the need for additional CFD simulations, significantly reducing computational costs and time. The integration of ML with CFD offers a promising solution to predicting supersonic fragment trajectories, allowing for more accurate and efficient modeling of complex aerodynamic interactions. Predicting supersonic fragment trajectories is a complex and nuanced problem, driven both by the nature of trajectory data itself and face dynamic interactions in high-speed environments. There are many challenges in forecasting accurate trajectories including the temporal properties that are multidimensional, high-volume trajectory data with trends and nonlinearity depending on the inherent complexities of the underlying movement [15]. Furthermore, the mixtures of traffic (e.g., pedestrian, car, and biker) create more complications in predicting trajectories between different classes [16]. Pedestrian trajectories have unique spatiotemporal characteristics, with increased degrees of freedom and complexity compared to vehicle trajectories making trajectory prediction tasks more challenging [16]. The ambiguity in predicting trajectories for the future makes this even harder, as we then need robust prediction models if predictions of a specific event have to cover multiple possibilities [17]. The difficulty that exists in trajectory prediction tasks is represented by dynamic social graphs, scene constraints, and global-local interactions; it must be addressed with

high priority [18]. The complexity and uncertainty emerging from the interactions among intelligent agents as well as agents with the environment make accurate trajectory prediction very difficult [19].

Finally, the fragment effecting from tracking failures like occlusion, drifting, and motion blur make trajectory prediction tasks more challenging to solve these issues and need highly reflective methodologies. The performance of trajectory prediction is dependent on sufficient context knowledge, history information about the target and surrounding entities must be integrated to overcome predictive challenges.

In the exampled field of aerospace engineering, predicting supersonic fragment paths becomes another problem with rapid part velocities and less distinct edge lines to outline what this thing will do once it comes apart. Compared to static point sources, the analysis of moving source data demands an additional accurate estimate of both temporal emission energy and trajectory which can easily amplify uncertainty for movement prediction [20]. In aerospace applications, trajectory prediction is even more challenging due to tracking failures such as occlusion and motion blur that make the trajectories end up fragmented requiring robust methods for this purpose [21]. Aerospace contexts, such as predicting the trajectories of fragments in the space environment where historical information and context are essential to improve prediction accuracy benefit from more sophisticated models considering that a fragment's trajectory is highly dynamic.

1.2 Limitations of Current Methods

The accurate prediction of aerodynamic forces for irregular fragments at supersonic speeds presents multiple challenges due to the limitations of both traditional experimental methods and computational techniques. Wind tunnel testing, although a long-standing method in aerodynamic research, is not well-suited for irregular fragments because it typically deals with regular, streamlined shapes. Irregular fragments, which often tumble during flight, cannot replicate their natural motion in the fixed orientations required for wind tunnel tests, resulting in incomplete and

inaccurate force measurements. Moreover, simulating supersonic conditions in wind tunnels requires highly specialized and costly equipment [11]. Ballistic range experiments provide more realistic free-flight data but struggle with the erratic behavior of irregular fragments, which makes it difficult to obtain repeatable and consistent results. Variations in surface area exposure during flight further complicate the measurement of drag forces, introducing uncertainties in the data. Additionally, maintaining and calibrating ballistic setups for supersonic speeds adds to the overall cost and technical difficulties [22]. Even Computational Fluid Dynamics (CFD), a powerful modern tool for simulating fluid dynamics, faces challenges when dealing with the complex geometries of irregular fragments. The need for high-resolution meshes and advanced turbulence models dramatically increases computational costs and time requirements. Non-linear interactions such as shock wave formation, boundary layer separation, and wake turbulence further complicate CFD simulations, making it difficult to guarantee accuracy under real-world conditions. The high cost and complexity of simulating supersonic conditions for irregular fragments limit the number of experiments and simulations that can be conducted, restricting the available data for analysis. As a result, developing generalized models to predict aerodynamic behavior remains a significant challenge. Each irregular fragment exhibits unique aerodynamic properties, which means that models must often be tailored to individual cases, limiting the applicability of broader predictions.

1.3 Literature Review

Supersonic fragmentation is a complex and multi-faceted process, which incorporates physical, chemical, as well as astrophysical processes that drive the destruction of material into smaller pieces. Numerical studies have shown that supersonic turbulence is a primary fragmentation trigger, producing shock compressions that induce the subsequent collapse of material [23]. Simulations of supersonic turbulence colliding with the interstellar medium at velocities similar to compressively driven magnetohydrodynamic shocks can create local density enhancements and promote fragmentation over a range of geometrical scales [24]. In the case of high-velocity micro-particle impacts, small fragments from a detonation were demonstrated to be

capable of producing injuries responsible for important tissue damage [25], reflecting well this destructive aspect of fragmentation events. In addition to this, it was found that there is an elongation of the core length due to which flow development characteristics may reorient, and such types of phenomena can result in fragmentation [26]. Suffice it to say, that the effects illustrate mechanical comminution of particle fracture pathways. Mobile drug delivery injectors utilizing hollow supersonic power nozzles have also been used as a method for dry powder injection. High-velocity impacts create shock waves that specialize in making fragmentation effects which permits crystalline powder particles to penetrate human skin membranes from the miniature version. These fragmentation processes are fundamental to many applications e.g. aerospace engineering, astrophysics, and pharmaceutical sciences where the dynamics of fragmentation significantly affect material behavior, structural damage, and impact events. Through a switching supersonic experiment in this study, we have shown that the fundamental processes of fragmentation phenomena are caused by some underlying mechanisms with important implications at many scales across disciplines. The subtleties of high-speed air flows could not even conceivably be meaningfully approached in any examination without a foundational understanding of the basic laws and concepts underlying supersonic aerodynamics, such as those governing shock waves, expansion fans, and boundary layers. Shock wave/boundary layer interaction (SWBLI), as one of the important physical problems in supersonic and hypersonic aerodynamics, has a direct impact on aero-applications like supersonic intakes and highly loaded turbo-machinery [27]. The Shock Wave-Laminar Boundary Layer Interactions (SWBLIs) phenomenon of shock waves and laminar boundary layers interacting in supersonic flows is an important aspect, influencing aerodynamic features such as skin friction drag and flow separation [28]. Explicit solutions for oblique shock and expansion waves can be developed from the quasi-one-dimensional nature of supersonic flows that have a strong effect on the aerodynamics behavior, it helps in obtaining efficient solution techniques [29]. These are essential solutions that help to understand the interactions between shock and expansion waves, which is important for proper aerodynamic optimizations of airfoils, wings, and other high-speed vehicles performing at supersonic conditions [29]. The ongoing difficulties in aerospace engineering regarding SWBLI phenomena are validated by

studying a high-order lattice Boltzmann flux solver to simulate shock wave/boundary layer interaction. The wave drag reduction techniques review in supersonic aerodynamics also observed that this same flow field achievement is aimed at sustainable supersonic travel for the aviation industry with active, passive, and hybrid control methods. The vortex lattice method has a long history in subsonic and supersonic aircraft aerodynamics, offering a general understanding of the flow dynamics. The discussion of basic ideas in supersonic aerodynamics that lies at the heart of the quick destruction or rapid transport downrange is part and parcel of a broad understanding of what happens when matter accelerates up to high velocity: Shock waves, expansion waves, boundary layers—these considerations give virtually everything that needs to understand what goes on inside high-speed fluid flow. Such complex supersonic flow phenomena can be investigated to understand and develop new aerodynamic solutions for fragments by using the rarefied regime. The other one talks about the essential concepts in supersonic aerodynamics which include the governing equations for supersonic aerodynamics such as Navier-Stokes Equations and Continuity Equation, Energy Equation, etc., to have a basic understanding of how high-speed airflow dynamics interact. [29] points out that the Navier-Stokes equations are a set of fundamental governing equations for fluid flow which includes momentum conservation, mass conservation, and energy balance in supersonic aerodynamics. These equations are integral in the ability to describe shock expansion and boundary layer interactions throughout highspeed flow, offering a well-versed foundation with which supersonic aerodynamic behavior can be assessed [29]. This is the continuity equation, which constitutes a basic law of physics in fluid dynamics and as such helps to explain how airflow inside supersonic flows behaves together with variations in the density for high-speed aerodynamic processes. Researchers, in supersonic aerodynamics, include the continuity equation and can predict flow patterns, shock wave interactions, and boundary-layer characteristics within high-speed airflow regimes. In supersonic aerodynamics, the energy equation is important for understanding the thermodynamic characteristics and heat transfer mechanisms that occur within fluid flow. The energy equation and the Navier-Stokes equations can be taken into account together to describe thermal effects, compressibility, as well as energy dissipation in supersonic flows which give information about the aerodynamic

performance [30]. The high-speed airflow included shock wave which was regarded as one of the most difficult sciences. The theoretical research must mainly depend on the Navier-Stokes equations, continuity equation, and energy equation for studying these shock wave phenomena. The use of these governing equations is demonstrated by the simulations conducted for investigating shock waves that prove to be significant in determining if all flow features (e.g. aerodynamic forces and boundary layer transition) can be accurately predicted or not, especially when dealing with high-speed aerodynamics applications [30]. For instance, the use of high-order numerical schemes built on Navier-Stokes equations and continuity equations has provided researchers with a powerful tool to study shock wave/boundary layer interaction in higher fidelity while improving computational efficiency. When these basic equations are included in computational fluid dynamics (CFD) simulations, researchers can investigate the stability of supersonic entropy layers and shock effects; as well as laminar-to-turbulent transition locations in hypersonic boundary layers to understand aerodynamic forces on a body and heating rates within it when designing hypersonics vehicles. |

[31] has detailed the investigation into the prediction of fragment parameters for conventional ammunition. The author collaborates on several methods for fragment mass and counts predictions, emphasizing alternative approaches from traditional Magis (original ensemble radiation model), Randers-Pehrson, and Stromse-Ingebritsen methods. Moreover, popular approaches in this field are Grady's model and Gold's methodology. The general form of methods for fragment prediction deals with cumulative fragment number, total number of fragments, and average fragment mass as well as a constant measure that weight in an unspecific way amount dispersion around fragment size. Further, [31] introduces a test data representation to visualize how individual parameter influences mass distribution inside the clump and provide a quantitative assessment of fragment properties. This study also evaluates the initial fragment velocity by the Gurney formula based on CAD data analysis of positions of projectile body fragments among different types at TTET. The article deals with diagnostics of fragmentation parameters for high explosive projectiles, and it emphasizes the appropriateness of describing mass distribution by Mott and Held

equations along with other effects made in continuation: influenceability of projectile body material on fragmentation process; action character assigned to high explosives raising. Further comparison of parameter sensitivity for different projectiles at the same time and several simulating resolutions is shown in [31], that piece compiled not only discrepancies over manufactured projectiles, B dimension or Λwithin resolved from tested rockets which have made sub-issues where expectations can not be utilized past simultaneously. These results imply that the non-physical constant B is more sensitive than the constant Λ and gives useful information about the spin influence on fragmentation parameters. This study greatly advances the characterization of fragments and prediction methodologies for fragment parameters in conventional projectiles to provide insights into important factors affecting their high-speed behavior. The Analysis of flow past irregularly shaped bodies like a fragment, which occurs as a result of the detonation by HEP with numerical simulations has been carried out in detail by [4] and includes pressure field distribution, velocity Field Magnitudes, Shock Wave formation around the object and streamline flows passing through these bodies. Its findings provide insights into the aerodynamic interactions involved in supersonic motion and how flow patterns, shapes, and resultant aerodynamic forces change for irregularly shaped fragments. In addition to this, [4]. This variable exposed surface area dictates the aerodynamic behavior of these fragments causing them to naturally shift from slender body form representation characteristic at high angle-of-attack and blunt body approximation in a low-angle flow field.

For example, the general aerodynamic models are applied to high-speed irregular bodies and limited application of specific aerodynamics models like the Spalart-Allmaras model on flows around a flying body [4]. Therefore, the results indicate that this model is capable of predicting aerodynamic performance in complex flows involving both boundary layers with strong pressure gradients and transonic flow phenomena. To further improve the accuracy of aerodynamic simulation in supersonic flows, researchers reveal that fragment dynamics can be better understood by using advanced models designed based on high-speed flow behavior. The study of [4] deals with the elements representative of irregular shapes, including viscous and

compressible flow effects, the dominance by pressure forces, the presence of shock waves, turbulent flow conditions as well as transient behavior in fluid behavior. The separation of the boundary layer from the body surface makes these aerodynamic interactions even more complex, emphasizing difficulties with predicting high-speed fragment trajectories and behaviors. This detailed investigation serves as a platform for further research of the aerodynamic intricacies involved in fragment motion during supersonic flow.

The use of the SU2 software to model transonic flow in a crooked channel is addressed by [32] describes the importance of keeping the Courant–Friedricks-Levy (CFL) number less than unity with grid refinement. An FGMRES algorithm is used for the linear solver in implicit formulations, and an error tolerance of 10-10 has been estimated to guarantee results down at least up to transonic flow simulations.

In addition, Ryabinin and Kuzmin investigated flow hysteresis in bent channels showing that there is an inherently unstable interaction of shock waves by recirculating/surging around sharp convex corners. Convective terms are integrated into the framework of the JST (Jameson-Schmidt-Turkel) scheme and the model requires a slope limiter proposed by [33] to improve higher-order convergence on cases with major shocks. Some advanced numerical schemes and turbulence models provide a systemic investigation for transonic flow in complex geometries. Ryabinin and Kuzmin present an example of using the SU2 open-source finite-volume solver to solve the URANS equations in unsteady transonic flows. Its work concentrates on 2D turbulent airflow in a twisted convergent-divergent funnel as the expulsion/swallowing of blast wave evolves along free-stream Mach numbers and examines flow topology inside channel/inlet entrance. To validate the obtained solution, it was solved numerically a lung airway model task that is motivated by an interesting study on problems of modeling outlet boundaries and cowl geometry impact on flow characteristics [32].

[32] uses high-speed Schlieren systems and numerical simulations to provide insights into the contraction ratio limits and flow characteristics at the beginning of intake operation. Comparison of solutions from various numerical solvers highlights the need for accurate discretization schemes and time-stepping methods in transonic flow

simulations.

[1]investigates arbitrary fragment geometry drag coefficient analysis in the hypersonic range with an emphasis on meshing sensitivity studies. [1] examines Mach numbers between Mach 3 and 7 on a numerically formulated arbitrary geometry fragment. The study identifies the force and moment coefficients in the x, y, and z directions, and also throughout trends are compared with theoretical expectations. The trend to the decrease in drag coefficients at higher Mach numbers is displayed by testing three orientations with unit vectors directed along principal axes, i.e., k,j, and j, i as per [1]. The study findings indicate that the results of aerodynamic quantities based on which was developed at lower hypersonic mach numbers, for example, Mach 3 could substantially inform about the behavior of aero properties at higher hypersonic mach number levels like Mach 5 and also even some extent with acceptable margin. An investigation of sensitivities realized as changes in grid space and normal extrusion parameters by the unstructured tetrahedral mesh used in simulation define drag effects. In the study, the authors further highlight experimental verification which includes wind tunnel testing and ballistic range experiments for decreasing errors to improve understanding of drag effects at higher Mach numbers [1].

Force and moment characteristics are meshing dependent but high Mach number results remain consistent overall. This research presents important findings in the aerodynamic performance of arbitrary fragment geometries at hypersonic conditions and can be used to inform trajectory prediction or airbreathing engine design for such high-speed environments. Its results are helpful for the estimation of drag coefficients and mesh sensitivity to fragment geometry, paving the way for further experimental validation [1]. A facility with a set of nozzles covering Mach 0.6 through to Mach 30 is used [34]. Each of the nozzle geometries is expressly designed to achieve perfectly homogeneous, core-isentropic laminar flow. The only study, referred to in the literature by many authors [35], offers a numerical one concerned with the interaction of cylinders located within the impingement region created by leading primary cylinder employing DSMC numerical simulations [34]. The research also investigates the implementation of a larger ring than nozzle outlet for disturbing flow prevention

purposes. The study additionally presents the difficulties in simulating shock wave shapes around spherical bodies moving through compressible transitional and slip flows. Although an analytical form is not available in this case, some empirically proposed expressions by [36] [37] allow the shape of a shock wave around a spherical body to be classified as having head or tail interactions. The research also indicates the codes developed by different space agencies, which reflect the importance of code development in terms of traditional space safety engineering [34]. Related work on changing dynamical properties and the need for updates of control laws and object models can be found in [38] with emphasis given to online correction via System Identification of the physical plant. This study alludes to the necessity for adaptable systems capable of handling a variety of operating conditions, and machine learning methods can be critical in attaining this adaptive capability within aircraft control systems. Moreover, [38]emphasizes the intricacies of motion control for modern aircraft due to a lack of awareness regarding parameters as well as potential flight regimes and environmental influences. Thus the study argues for a compensation of control systems in case of; failure equipment, damaged structure, and abnormal flight situations by updating dynamically the feedback gains. The research illustrates the hardships in high-speed flight scenarios through adaptive control using neural network modeling and control them. The study examines neural network system identification methods for modeling nonlinear systems and points out how artificial neural networks can be specified to have universal approximation capabilities. [38] commits that neural networks are a poor tool when it comes to representing highly-dimensional dynamical systems with few variables readying modeling approach applications for handling ever-growing complex control problems. The research demonstrates the efficiency of adaptive models in built-in management techniques such as the Model Reference Adaptive Control (MRAC) technique to boost the adaptiveness of the management system [38]. Using machine learning methods, this article examines the motion control of supersonic passenger aircraft thus providing insights into adaptive control, along with system identification and neural network implementation in aerospace engineering. These results provide implications for improving control systems' adaptability and performance in dynamic flight environments, which will help us to better understand adaptive control strategies on high-speed aircraft. In the

specific example of space debris, those aerodynamic forces must be modeled for interacting spheres during re-entry, and [3]focuses on a supersonic rarefied wind-tunnel environment. Another study has shown that shock/shock interaction behaves quite differently relative to the continuum regime in rarefied regimes containing thicker and more diffuse shock waves where it is challenging to explore pressure and heat flux distributions. The article [3] reveals the experimental arrangement with spheres in a supersonic rarefied wind tunnel that is illustrated to investigate detailed aerodynamic features addressed from re-entry conditions of space debris. This research investigates the pressure distribution and heat flux as a result of interaction between spheres in hypersonic, rarefied flow conditions which would help to understand more about aerodynamic forces due to different factors acting on winds around this kind of atmosphere. In addition, the investigation presents a comprehensive study of complex shock wave interactions around spherical bodies in compressible flows over transitional and slip regimes. Analytical formulations for such cases are sparse; however, Cardona and Lago propose empirical expressions in rationalizing the shapes of shock waves around spherical bodies in rarefied regimes. This research is significant for guiding the understanding of shock wave behaviors and effects on aerodynamic coefficients in high-speed flow conditions. Likewise, experimental validation becomes paramount in the context of understanding aerodynamic forces and heat flux levels for rarefied flow regimes [3]. This unsolved enigma increases the uncertainty in space safety engineering and debris management, towards which our knowledge should move forward; for that purpose, a study is carried out here aimed at improving understanding of aerodynamic interactions among fragmented fragments during re-entry by using experiments with supersonic rarefied wind-tunnel setups. The work tackles the development of a compressibility model to predict aerodynamic forces that act over non-regularly shaped bodies like fragments from a high-explosive projectile [39]. The work is based on a general model for the nonlinear prediction of aerodynamic forces and moments with triaxial ellipsoids as representative shapes. The presented model is the next step of the work done by one author in previous years towards estimating the area to which sides of different shapes are exposed during its travel, and it is used for estimation trajectory parameters when non-standard body shapes exist. Abide by the approach in numerical

simulations for ellipsoids and refer to the previous work of the author in detail on the methodology employed for fragments. This is shown by the figures of simulations for flow along positive and negative y and z axes [39]. The study estimates pressure near the fragment surface considering adiabatic changes in the gas state due to the rapid motion of the sample relative to heat transfer processes and calculates specific volume and air compression values at different positions. Kljuno and Catovic pay more attention to determining the forces acting on a body by calculating aerodynamic force as the law of momentum change (like Newton's model for hypersonic motion). The integration of that expression means multiplying it with a planar angle and integrating over x- and y-coordinates at the plane into which the fragment is projected, where regions of fragmentation are supplemented by ellipse half-axes. This method of calculation allowed the determination of work, i.e., adiabatic compression per fragment [39]. Also, the compressibility model proposed by [39] is adopted to estimate aerodynamic forces acting on non-spherically shaped bodies due to adiabatic air compression in front of hypersonic fragments. It exhibits the capability of this model to decrease relative error in modeling aerodynamic forces for high-velocity fragments with a significant degree of air compression, by comparing results obtained through numerical simulations and experimental data. Gerasimov et al. are focusing on the aerodynamics of cube fragments in high-speed air medium [40]. The study provides numerical simulations and experimental research in which the focus is on the supersonic flow around cubic fragments oriented at different angles to the incoming flow vector. Thus, the visualization of a supersonic flow around cubic-shaped bodies was carried out by Gerasimov et al., where two methods were presented for this purpose: theoretical — with consideration of numerical solutions to multidimensional mathematical models; and experimental shadow photo capture. The realization of external gas flow around the cube is achieved by using an applied 3D numerical calculation to account for boundary conditions on the surface of the cubic body and the computational domain walls. The study uses the full Reynolds-averaged Navier-Stokes equations with a two-parameter turbulence model to interpret the flow features. The research uses the ideal gas state equation for air in simulations, where a wide spectrum of initial flow velocities is considered constant from 2 to 10 Mach numbers. Besides that, [40] points out the necessity of using reliable controlled work

models (CWM) as well the ground test methods in air aerodynamics shooting galleries for scientific research and mapping to appropriate life-sized studies object properties during free flight. The way it's carried out means test objects are catapulted from powder, or light-gas installations with defined speed and angle of attack. During the flight, optical tools determine the positions of the object being test-flown at certain fixed time intervals to find out center-of-mass coordinates. This research highlights the particularities and constraints implied in the case of small bodies (fragments) as compared to common aerodynamic tests for regular-sized structures. The work of [40] also provides a better comprehension of aerodynamics around irregularly configured bodies at high-speed air-flowing conditions. The research reveals information flow properties, pressure field distributions, and aerodynamic forces of supersonic/hypersonic cube-shaped fragments by coupling between numerical simulations and experimental investigations. The new study could make a difference in applications for aerodynamics analysis trajectory prediction and aerospace engineering under high-speed conditions. Among these [41] aim to formulate the drag correlation for non-spherical rough particles. Geometric drag models are calibrated and validated through an inverse design analysis to improve the accuracy of isometric non-spherical particle drag prediction with sphericity as a shape parameter described. Some of the fragments employed in the study are shown inFigure 1.1. In the positive y direction, one unique correlation law becomes possible for normalizing the particle drag coefficient concerning that of a sphere and another allows this drag correlation formula to be used over most Reynolds numbers [41]. This new experimental data taken properly into account improves the accuracy and range of applicability of this formula, hence it gives a better understanding of drag force for non-spherical particles. [41] also discusses the implications of the drag correlation formula in both practical applications, such as in industrial processes for chemical engineering, and natural phenomena, like the settling patterns of solid inertial particles in riverbeds. It can be seen that, due to the formula's consistent estimation of drag forces at various Reynolds numbers and particle shapes, it is important in numerous research areas as well as practical applications.

Dioguardi and Mele note that proper shape descriptors and correlation laws are

crucial when predicting the drag force on non-spherical particles. It considers shape dependence in drag coefficients and provides a detailed tool to predict the forces that are expected over non-spherical rough particles [41]. Dioguardi and Mele note that proper shape descriptors and correlation laws are crucial when predicting the drag force on non-spherical particles. It considers shape dependence in drag coefficients and provides a detailed tool to predict the forces that are expected over non-spherical rough particles [41].

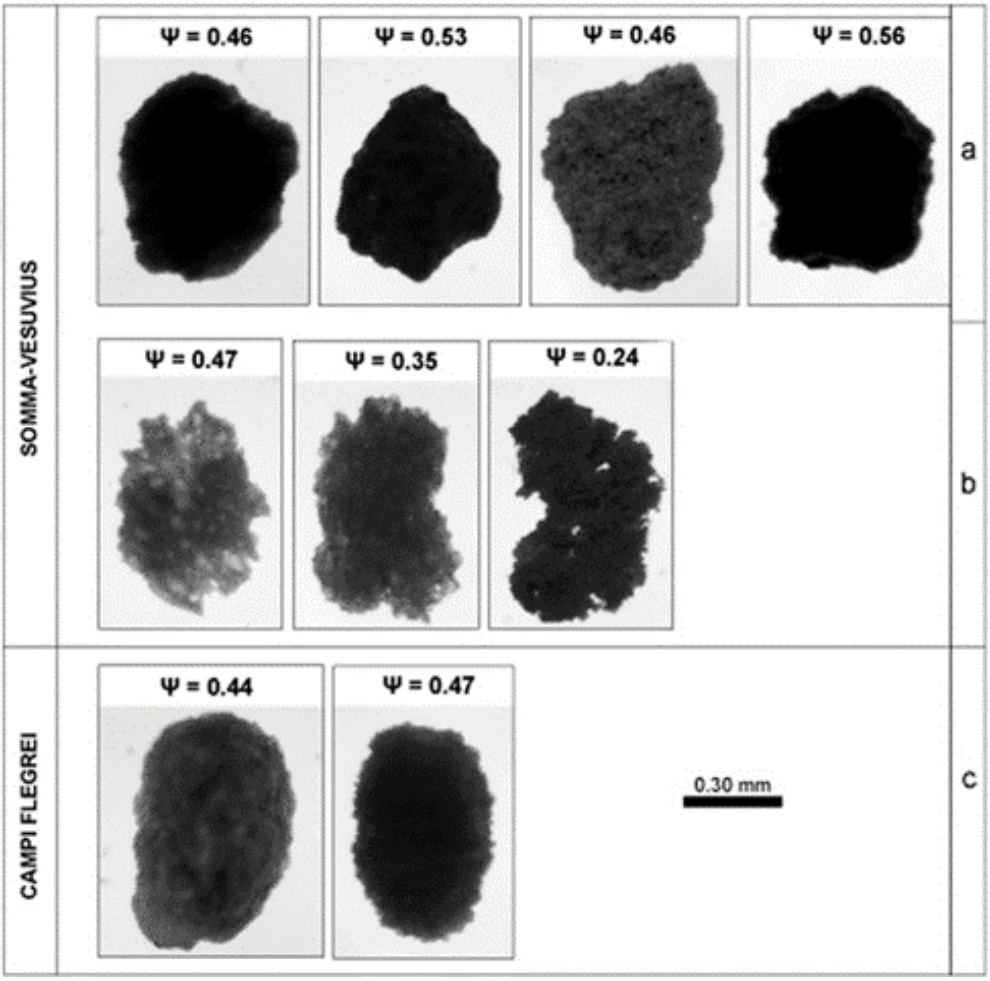

Figure 1.1 These are some of the fragments used in this study [41]

Dioguardi and Mele note that proper shape descriptors and correlation laws are crucial when predicting the drag force on non-spherical particles. It considers shape dependence in drag coefficients and provides a detailed tool to predict the forces that are expected over non-spherical rough particles [41].

[6] aimed at developing an ANNs-based surrogate drag model specially built for non-spherical fragments of explosive canvases was published. This work tries to

improve the accuracy of drag predictions for non-spherical particles with other machine-learning algorithms. The work by Xin et al. studies an additional function, “blending”, that is incorporated into one drag correlation formula for fragments whose shape are non-spherical; though various shapes differing from Mach number require extensive validations.

Additionally, the study investigates how this "blending" affects fragment drag coefficients at high Mach numbers and therefore furthers our understanding of when it is applicable across various flow regimes. This paper addresses the intricacy of creating orientation-dependent drag coefficients and explores alternative ways to drag coefficients for an irregular non-spherical fragment; this led them to propose a weighted average approach, where each particle is split into several sub-spheres [6]. They also investigate how the drag coefficient is Reynolds-averaged about fragment shape across subsonic as well as supersonic motion regimes, it shows a fragment, as well as its CAD form and meshed shape in **??**. So, they propose corrections on a sphere drag correlation based on geometry and attempt to obtain better results of the estimation for drag coefficient values under different flow conditions concerning non-spherical particles.

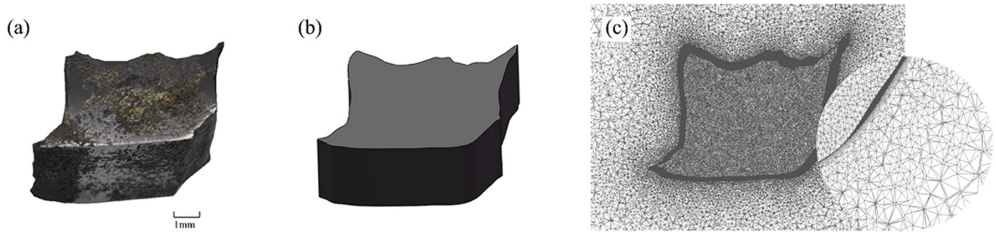

Figure 1.2 a) A fragment that is used in this study. b) CAD design of the fragment. c) The fragment after meshing is done [6]

The study also investigates the use of a "blending" capability to track orientation-dependent drag coefficients for non-spherical fragments. In a high-speed flow environment, [6] studied the effects of drag forces on different fragment orientations by considering characteristic drag coefficients in axial and cross-flow directions. They present a new method for predicting the drag force on non-spherical fragments and provide very interesting results in estimating correlations of drag coefficients with complex particle shapes. A more focused version on machine learning techniques and the drag model depending on shapes used in CFD simulations

can greatly expand our knowledge of aerodynamic forces acting inside non-spherical fragments, which helps a lot for fluid dynamics advances with particle analysis too. This model is further calibrated and implemented to study the drag coefficient of volcanic ballistic projectiles (VBP) originating from Popocatépetl volcano in Mexico. As an answer to this limitation, more than 40 published or submitted papers have dealt with the dispersion and emplacement of VBP fragments over the terrain [42] looking at considerations regarding drag coefficient which is a very important parameter in understanding trajectories as well as behavior of these particles. The experimentally determined drag coefficients in [42] demonstrate the importance of an accurately calibrated model for the correct calculation of volcanic plume behavior. The research aims to improve the accuracy of trajectory predictions and range estimations for VBP within volcanic terrains, by calibrating this model with Popocatépetl volcano projectile features. In the case of VBP irregularly shaped flaked (flax and grass with a modified shape), drag coefficients for each separate chip were used to maintain mechanical homogeneity (firmness) instead of a constant coefficient of 1. The study attempts to understand the effect of shape-dependent drag correlations on precision cushioning computation and impact evaluation for VBP [42] In addition, this research has critiqued the maximum range calculations using their calculated drag coefficient and thus emphasized how new accurate values of evaluated coefficients must be exploited to suitably estimate VBP paths. As such the study by [42] suggests a better result and closer to field measurements, compared with a constant coefficient of 1 value using shape-dependent drag coefficients approached in this work. The findings contribute to a better understanding of the drag forces on non-spherical particles and their role in impact dynamics as well as safety assessments for building structures in volcanic areas. In [43], the aero-optics characteristics have been investigated for two bodies in supersonic flow, and attention has particularly focused on the collimation of resistance associated with the disturbance inside the wake produced by the front body. The findings illustrate the complex behavior of such bodies, specifically what is known as the collimation effect (where a smaller body gets sucked into the wake behind another). Moreover, the study confirms that a disturbed region behind an incident body with lower resistance represents when faced by high-speed flow fields for understanding the aerodynamic behaviors of fragments. [43] investigates two

round-nosed bodies at close separation, focusing on the collimation effect and drag forces of the forward body. According to the study, this collimation effect causes them to move together with zero separation between their bodies. It reveals differences in the expression of collimation according to body size ratio, which can be understood as information on the aerodynamic interaction among SH fragments with supersonic flow [43]. [43] applies a combined aerodynamic and dynamic approach to study the flow around two spheres close to each other in radius. Parameters such as the aerodynamic coefficients and the spheres' trajectories enable a depiction of the dynamics of the force field at work during the movement of bodies. The research highlights the necessity of precise identification of the aerodynamic characteristics of bodies in the supersonic flow as well as the complexity of including them in the dynamic picture. The study provides relevant investigations regarding the aerodynamic qualities and dynamic interactions of bodies and the effect of collimation, drag forces, and calculation of trajectories in high-speed flow conditions. This research serves to contribute to the understanding of aerodynamic qualities, the interaction of fragments, and their later applications to aerospace facilities and the study of impact dynamics 2. An alternative study by (Li et al., 2015). reports on the actions of fragments in high-speed flow. The research builds on the concepts of supersonic flow based on previous literature. The study explains the precision of the numerical model as well as the computational performance through the comparison of the outcomes of the experiments to Numerical simulations. The underlying experimentation undertaken by (Laurence et al., 2012) in the area of separation of two spheres is considered when referring to different radios and locations, and it adds value to the associated bodies studies. [44] also account for the complications brought about by the flows with both turbulence and shocks and the approximate methods used to simplify the dynamics. The study explains the effects of integration based on the adaptive mesh refinement, which must handle the unsteady images and, hence, must retain the grid perfectly for a smooth calculation [44]. The work of [44] also studies how to enforce immersed boundary conditions via the ghost fluid method due to its ability to be coupled with level sets. The author successfully enforced immersed boundary conditions for complex moving boundaries [44] and explained the details involved in this process. [44] further enhances our understanding of aerodynamics and

fragment-fragment interactions while providing insights relevant to aerospace.

1.4 Objectives of the Thesis

Estimating coefficients of lift and drag on nonconforming shapes used in fragmenting warheads. In this study, we consider the aerodynamics of a fragment released from a warhead as it impacts different Mach numbers based on an open-source CFD solver. The Mach numbers investigated in this work are 0.8, 1.0, and 1.2, corresponding to the subsonic, transonic, and supersonic flow ranges, respectively. These orientation-specific flow fields are then used to calculate the aerodynamic interactions due to the fragment's irregular form during an investigation that concentrates on 30 different angles of orientation. This shape model is derived from real life using empirical data from defense industry tests in Türkiye. The CFD simulations were performed by solving the Reynolds Averaged Navier-Stokes (RANS) equations, which are considered very convenient in terms of modeling a turbulent flow regime. The solutions are obtained assuming a steady state, with turbulence modeled using the Spalart-Allmaras model modified by including an extended wall function (EWF) for improved all-wall treatment. By this approach, a better estimation of how the flow behaves over the surface of that particular piece is converged which appears to be very important for getting aerodynamic forces i.e., lift and drag started. In this thesis, an attempt is made to study the aerodynamic behavior of non-spherical fragments for 30 different orientations in a supersonic flow field at Mach numbers 0.8, 1.0, and 1.2. This work will provide the drag coefficient, calculations of drag forces, and exposed areas for all the orientations against a comparative assessment of C_D profiles and the effect of orientation and geometry on the aerodynamics performance. The main point of this analysis will be a comparison of three important values of $C_D$the average $C_D$obtained over the 30 orientations, the value of $C_D$derived from the relationship between the average drag force the average exposed area, and the C_D of a geometrically obtained shape derived from the averaged coordinates themselves. This comparison aims to emphasize the efficiency and practicality of using average $C_D$values in aerodynamic modeling to reduce computational time. It also discusses the use of average C_D values in trajectory calculations so that a balance between

computational simplicity and predictive accuracy is obtained. It presents how the usage of average $C_D$can simplify real-time analyses, keeping in mind the possible deviation of such methods from the results of the individual orientation-specific analysis. This study further integrates advanced predictive techniques to investigate variability in C_D at different orientations and to realize efficient yet accurate aerodynamic predictions. The integrated approaches discussed here contribute to an understanding of fragment dynamics within supersonic regimes and provide modeling improvements for trajectory predictions within hazard assessments related to safety-critical applications.

1.5 Structure of the Thesis

The subject of this thesis is difficult to study in detail mainly because the aerodynamics of supersonic fragments cover different flow conditions that make it hard to predict their trajectory. The research is framed to overcome some of the basic shortcomings in existing techniques followed for path prediction and it endeavors as well to add value by performing a comprehensive numerical quantification employing Computational Fluid Dynamics (CFD).

The thesis starts with a comprehensive review of the literature on predictive engineering in predicting trajectories of supersonic fragments. The review will provide the groundwork for identifying knowledge gaps and areas warranting additional inquiry.

At the heart of this study is to use of a CFD solver simulating supersonic fragmentation flow. The modeling is carried out within the well-defined computational domain and the CFD model contains both, governing equations for fluid dynamics in a physical context. Particular attention is dedicated to the solver setting and corresponding turbulence model, which has been selected based on its relevance in this work (Spalart-Allmaras).

To guarantee the accuracy and stability of simulations, boundary conditions as well as flux discretization methods are also discussed. Following the simulation, a mesh independence study is conducted to confirm that results are not significantly influenced

by grid size.

This thesis studies the influence of different orientation angles concerning the freestream on the aerodynamic behavior of fragments and how this angle affects flow fields and corresponding aerodynamic forces. Flow fields are calculated, analyzed, and interpreted to conclude how fragments behave under different conditions.

On the whole, finally, the thesis is surrounded by:

Challenges of simulating the trajectories of supersonic fragments and ways to mitigate them. Assess existing methods and new developments to resolve the limitations using high-fidelity CFD techniques. The mesh independence test will be carried out to ensure valid numerical results. Study of the orientation angles influence in aerodynamic performance at supersonic fragments. Study of computed flow fields to study the effect of different flight conditions on fragment behavior. This holistic approach can lead to a better understanding of the aerodynamic behaviors of the supersonic fragments and it may help predict performance in terms, that might be useful for supporting solutions for design or control purposes if these kinds of objects are considered in practical cases.

1.6 Scope of the Thesis

The scope of this thesis is an investigation of the aerodynamic characteristics of non-spherical fragments over a range of Mach numbers 0.8, 1.0, and 1.2. In computing C_D, drag force, and exposed area for a total of thirty different orientations at each of the Mach numbers, the current study has attempted to capture the variation in the performance of aerodynamics caused by shape and orientation.

Averaged C_D values for trajectory simplifications and calculations of specific orientation-based C_D are performed in the thesis, enabling a fine-grained understanding of the aerodynamic forces for various conditions.

The study further includes the potential benefits of geometrical optimization by comparing optimized shapes with the original fragment to assess the reductions in C_D

and drag force. This provides a balance between practical applications using average drag coefficients for simplified, real-time trajectory calculations and investigates the computational trade-offs when more precise, orientation-specific models are required. It further discusses the extent to which advanced predictive models, such as surrogates using machine learning algorithms, can enable drag prediction to be run on lesser computational resources. These results are likely to be useful in explosion safety, aerospace engineering, and defense industries that require highly accurate trajectory analysis and aerodynamics evaluation with valuable insights related to developing powerful, flexible modeling approaches under safety-critical environments.

CHAPTER 2

NUMERICAL METHOD

2.1 CFD Solver

As a CFD solver SU2 (Stanford University Unstructured) has been used, which is an open-source collection of software tools written in C++. SU2 solves the Reynolds-Averaged Navier-Stokes equations (RANS) using the finite volume method, with all results presented in non-dimensional form, allowing for comparison across various flow conditions. SU2 is capable of conducting numerical simulations of the three-dimensional, compressible/incompressible, turbulent/laminar, steady/unsteady flows.

2.2 Computational Domain

Prism cell layers have a fixed growth rate of 1.2 and the number of boundary layers is adjusted to obtain the approximated total thickness. The hybrid-grid structure is illustrated in Figure 2.1, where prism cells are rendered in red and tetrahedral cells are shown in green color. A typical hybrid mesh around the fragment is shown in Figure 2.2. The fragment is shown in Figure 2.3. The basic numerical grids used in the present investigation were of unstructured hybrid meshes consisting of different cell patterns to be adapted for proper analysis. In this case, prismatic cells were utilized to resolve the boundary layer and hence correctly model the gradient in normal-to-the-wall locations while tetrahedral mesh gave a balance between the accuracy of solving versus solution time for a flow field domain. The fragment was sampled on the surface by triangular elements and used for a detailed geometric representation of complicated fragment shapes as shown in Figure 2.1 and Figure 2.2.

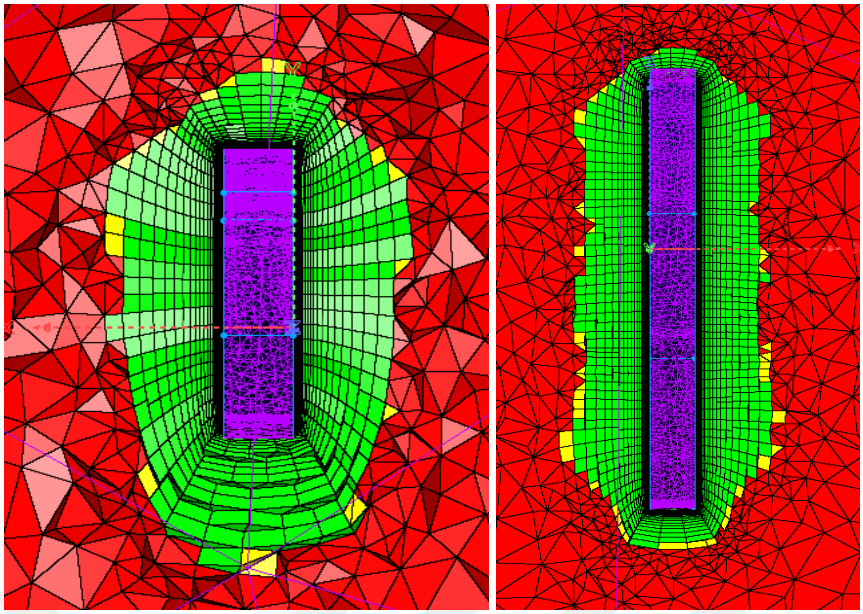

Figure 2.1 Typical view of the refined mesh

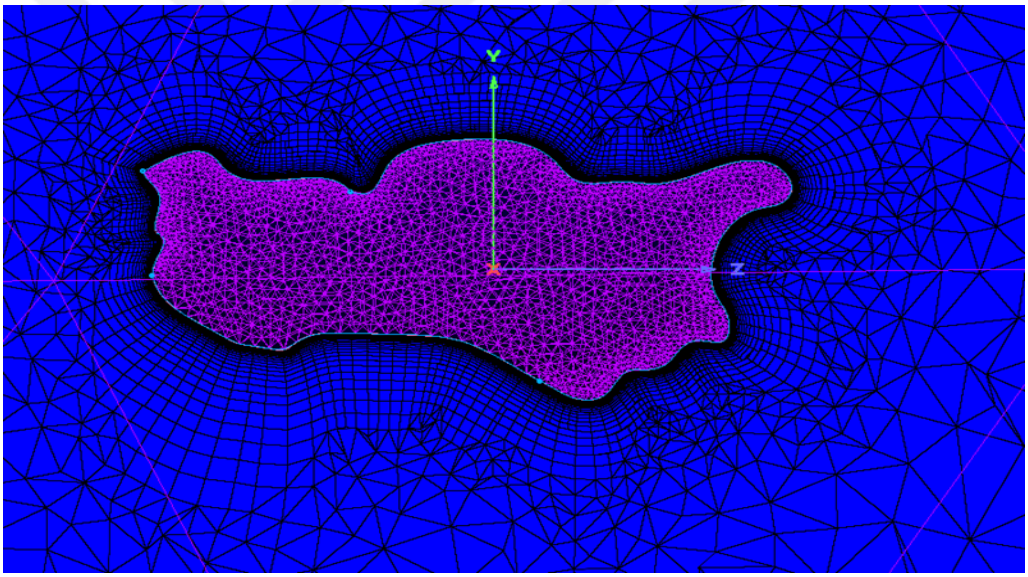

Figure 2.2 Typical hybrid mesh around the fragment

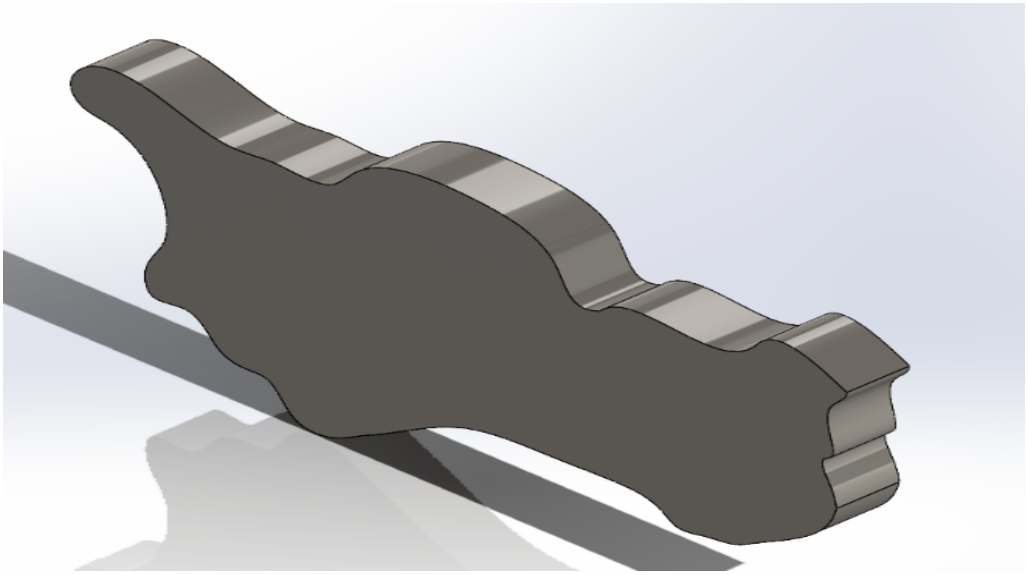

Figure 2.3 Fragment

2.3 Governing Equations

The Reynolds-Averaged Navier-Stokes equations mathematically establish a compressible flow's mass, momentum, and energy conservation principles. The governing equations in the integral form are as follows:

$$\frac{\partial}{\partial t}\int_{\Omega} U d\Omega + \oint_{S}\left(\vec{F_c}(U) - F_v(U)\right)\cdot\vec{n}\cdot ds = 0 \qquad (\mathbf{2.1})$$

U is the flow variable vector in conservative form, $\vec{F_c}(U)$ and $F_v(U)$ are the convective and viscous flux terms, respectively. The volume integral denotes integration over the control volume Ω and the surface integral is computed over the control surface. Here the volume integral means that integrates on control volume over the Ω and the surface integral is calculated for the control surface. The flow is solved by employing the finite volume method to discretize SU2 governing equations.

Convective and viscous flux vectors, when applied to a three-dimensional issue, are defined as

$$U = \begin{bmatrix} \rho \\ \rho v_x \\ \rho v_y \\ \rho v_z \\ \rho E \end{bmatrix} \qquad (\mathbf{2.2})$$

ρ is the density, v_x, v_y, v_z is the velocity component, and E is the energy per unit mass.

The RANS equations are widely recognized and extensively employed in analyzing compressible and turbulent flows. Understanding this framework not only enhances the study of fluid mechanics but also contributes to advancements in engineering solutions. Convective fluxes contain three fluxes.

$$\overrightarrow{\overrightarrow{F_c(U)}} = \overrightarrow{F_{c_x}}(U) + \overrightarrow{F_{cy}}(U) + \overrightarrow{F_{c_z}}(U) \tag{2.3}$$

$$\overrightarrow{F_{c_x}} = \begin{bmatrix} \rho v_x \\ \rho {v_x}^2 + p \\ \rho v_x v_y \\ \rho v_x v_z \\ \rho v_x H \end{bmatrix}, \quad \overrightarrow{F_{c_y}} = \begin{bmatrix} \rho v_y \\ \rho v_x v_y \\ \rho {v_y}^2 + p \\ \rho v_y v_z \\ \rho v_y H \end{bmatrix}, \overrightarrow{F_{c_z}} = \begin{bmatrix} \rho v_z \\ \rho v_x v_z \\ \rho v_y v_z \\ \rho {v_z}^2 \\ \rho v_z H \end{bmatrix} \tag{2.4}$$

p is the static pressure and H is the flow enthalpy which is defined as $H = E + \frac{p}{\rho}$

The viscous fluxes are defined as follows,

$$\overrightarrow{F_{v_x}} = \begin{bmatrix} \tau'_{xx} \\ \tau_{xy} \\ \tau_{xz} \\ \Theta_x \end{bmatrix}, \quad \overrightarrow{F_{v_y}} = \begin{bmatrix} \tau'_{xy} \\ \tau_{yy} \\ \tau_{yz} \\ \Theta_y \end{bmatrix}, \quad \overrightarrow{F_{v_z}} = \begin{bmatrix} \tau_{xz} \\ \tau_{yz} \\ \tau_{zz} \\ \Theta_z \end{bmatrix} \tag{2.5}$$

$$T = \begin{bmatrix} \tau_{xx} & \tau_{xy} & \tau_{xz} \\ \tau_{yx} & \tau_{yy} & \tau_{yz} \\ \tau_{zx} & \tau_{zy} & \tau_{zz} \end{bmatrix} \tag{2.6}$$

The viscous stresses can be defined as

$$\tau_{ij} = \mu_{tot} \frac{\partial v_i}{\partial j} + \frac{\partial v_i}{\partial i} - \frac{2}{3} \delta_{ij} \nabla \vec{v} \tag{2.7}$$

Where $\nabla \vec{v}$ is the divergence of the velocity, δ_{ij} is the Kronecker delta function

$\mu_{\text{tot}} = \mu_{\text{dynamic}} + \mu_{\text{turbulent}}$.

μ_{dynamic} is presumed to assure Sutherland's Law

while $\mu_{\text{turbulent}}$ is determined by using turbulence models

$$\frac{DW}{Dt} = \nabla\vec{v}\tau_{ij}$$
$$\frac{DQ}{Dt} = \mu_{tot}{}^{*}\mathrm{C}_p\nabla T \quad \textbf{(2.8)}$$

C_p is the specific heat constant and $\mu^*_{\text{tot}} = \frac{\mu_{\text{dynamic}}}{Pr_{\text{dynamic}}} + \frac{\mu_{\text{turbulent}}}{P_{\text{turbulent}}}$

$$\theta_x = v_x\tau_{xx} + v_y\tau_{xy} + v_z\tau_{xz} + \mu^*_{\text{tot}}\, C_p\frac{\partial T}{\partial x} \quad \textbf{(2.9)}$$

$$\theta_y = v_x\tau_{yx} + v_y\tau_{yy} + v_z\tau_{yz} + \mu^*_{\text{tot}}\, C_p\frac{\partial T}{\partial y} \quad \textbf{(2.10)}$$

$$\theta_z = v_x\tau_{zx} + v_y\tau_{zy} + v_z\tau_{zz} + \mu^*_{\text{tot}}\, C_p\frac{\partial T}{\partial z} \quad \textbf{(2.11)}$$

2.4 Solver Setup

In this study, flow is described using steady-state Reynolds-averaged Navier-Stokes (RANS) equations with S-A turbulence models. Convective fluxes like momentum and energy mass are estimated by a finite difference scheme, JST (Jameson-Schmidt Turkel), and Green-Gauss methods are used for gradient calculations of flow variables such as velocity, pressure, and temperature. Although the flow field is described using steady-state equations, the system must still be discretized in time. The study leverages an implicit Euler method for temporal discretization. In addition, the local-time stepping is also used in SU2 to accelerate the convergence. The implicit problem is solved using the Flexible Generalized Minimal Residual (FGMRES) method with Incomplete Lower Upper (ILU) factorization.

2.5 Turbulence Model

The Reynolds number, a crucial factor in identifying whether a flow is laminar or turbulent, determines whether the flow is viscous or laminar. The following formula is used to determine the Reynolds number (Re):

$$\mathrm{Re} = \frac{\rho \cdot \mathrm{U} \cdot \mathrm{L}}{\mu} \tag{2.12}$$

Re is Reynolds number, ρ is the fluid density, U is the velocity of the fluid flow, and L is the characteristic length, μ is the dynamic viscosity. The air is considered to be laminar if the Reynolds number falls below 500.000. The flow is primarily viscous (in layers of adjacent ordered flows) and laminar. The flow is called turbulent for air when the Re exceeds 10^6. Flow shows a completely random motion, eddy, and mixing phenomena due to time inertial forces dominating. Where the flow has a transition phase from streamlined to turbulent if the Reynolds number is between 500.000 – 1.000.000.

In CFD analyses, turbulence models must be employed to model the influence of Reynolds number on turbulent flows. Reynolds-Averaged Navier-Stokes (RANS) equations and different turbulence models like Spalart-Allmaras, $\mathrm{k} - \varepsilon$, or using a hybrid-wall function.

The turbulence model used for the Navier-Stokes equations is fundamental to mathematically modeling how flow behaves as it becomes more turbulent. In fluid dynamics, turbulence or turbulent flow is the motion of particles in a unified manner that results from nature and has intense movement with great power. The use of flow solvers based on the Navier-Stokes equations in conjunction with a turbulence model would mean that turbulent fluctuations could be included and make it possible to predict what can happen regarding fluid behavior.

Selecting the Spalart-Allmaras turbulence model is efficient and relatively accurate in predicting turbulent flows. Spalart-Allmaras model — suitable for low-Re turbulence, providing accurate results with a less computational cost. This is also especially well-suited for the study of fragment aerodynamic characteristics because it is known

to handle reliable success turbulence effects and has been verified in many other different analyses. Also, the Spalart-Allmaras model has shown to be reliable in various aerodynamic applications and validated concerning experimental data; it is well known that accurately captures the turbulence effects on fragment behavior.

Consequently, any simulation of turbulent flows provides zero value without the turbulence model in Navier-Stokes equations such as Spalart-Allmaras and insight into aerodynamics behavior due to fragments under a variety of flow cases.

2.6 Spalart-Allmaras Governing Equation

The turbulent viscosity term in this paper is calculated by the one-equation turbulence model, the Spalart–Allmaras (SA) model. The SA model is widely used in numerical analysis to give accurate and reliable results. The Near Wall region and finite Reynolds Number are from the initial study by [45].

$$\nu_t = \tilde{\nu} f_{v1}, \quad f_{v1} = \frac{\chi^3}{\chi^3 + C_{v1}^3}, \quad \chi \equiv \frac{\tilde{\nu}}{\nu}, \quad \mu_t = \rho \nu_t \tag{2.13}$$

ν is molecular viscosity and $\tilde{\nu}$ obeys the transport equation,

$$\frac{D\tilde{\nu}}{Dt} = c_{b1}\tilde{S}\tilde{\nu} + \frac{1}{\sigma}\left[\nabla((\nu+\tilde{\nu})\nabla\tilde{\nu}) + c_{b2}(\nabla\tilde{\nu})^2\right] - \left[c_{w1} f_w\right]\left[\frac{\tilde{\nu}}{d}\right]^2 \tag{2.14}$$

where

$$\tilde{S} \equiv S + \frac{\tilde{\nu}}{\kappa^2 d^2} f_{v2}, \quad f_{v2} = 1 - \frac{\chi}{1 + \chi f_{v1}} \tag{2.15}$$

$$f_w = g\left[\frac{1 + c_{w3}^6}{g^6 + c_{w3}^6}\right]^{1/6}, \quad g = r + c_{w2}\left(r^6 - r\right), \quad r \equiv \frac{\tilde{\nu}}{\tilde{S}\kappa^2 d^2} \tag{2.16}$$

The constants of the following equations are,

$$c_{b1} = 0.1355, \quad \sigma = \frac{2}{3}, \quad c_{b2} = 0.622, \quad \kappa = 0.41,$$
$$c_{w1} = \frac{c_{b1}}{\kappa} + \frac{1 + c_{b2}}{\sigma}, \quad c_{w2} = 0.3, \quad c_{w3} = 2, \quad c_{v1} = 7.1 \tag{2.17}$$

At the wall, the boundary condition $\tilde{\nu} = 0$ is applied, while at far-field, Spalart Allmaras suggests a finite value for $\tilde{\nu}$ which is below $\nu/10$. Equation 2.13 is implemented in the code as the convective, viscous, and source terms follow:

$$\vec{F}_c = \vec{v}\tilde{\nu}, \quad \vec{F}_v = \frac{\nu + \tilde{\nu}}{\sigma}\nabla\tilde{\nu}, \quad Q = c_{b1}\tilde{S}\,\tilde{\nu} - [c_{w1} f_w]\left[\frac{\tilde{\nu}}{d}\right]^2 + c_{b2}(\nabla\tilde{\nu})^2 \tag{2.18}$$

2.7 Boundary Condition

The solution of the flow with the SU2 program requires some boundary conditions to be correctly defined while modeling. No slip and far-field are the most common basic boundary conditions used during simulations.

The no-slip boundary condition would be the best turbulence boundary to be considered if fragment aerodynamic parameters are to be calculated. No slip is the boundary condition used at solid boundaries, which is taken as a wing surface, any fragment, or any solid object embedded in the flow. This means that the fluid has no velocity concerning the boundary. To explain it better, say at a solid object's surface, the fluid velocity is the same as that of the object's physical velocity. For a solid object, it means the flow velocity of the fluid at the surface is zero. No slip boundary condition is applied to the fragment.

The fragment was created as a far-field at 20 times its characteristic lengths and the other edges were created with around 10 times on them. The conventional far-field boundary conditions have been applied for each of the fragments. No slip and far-field

boundary conditions are as shown in Figure 2.4.

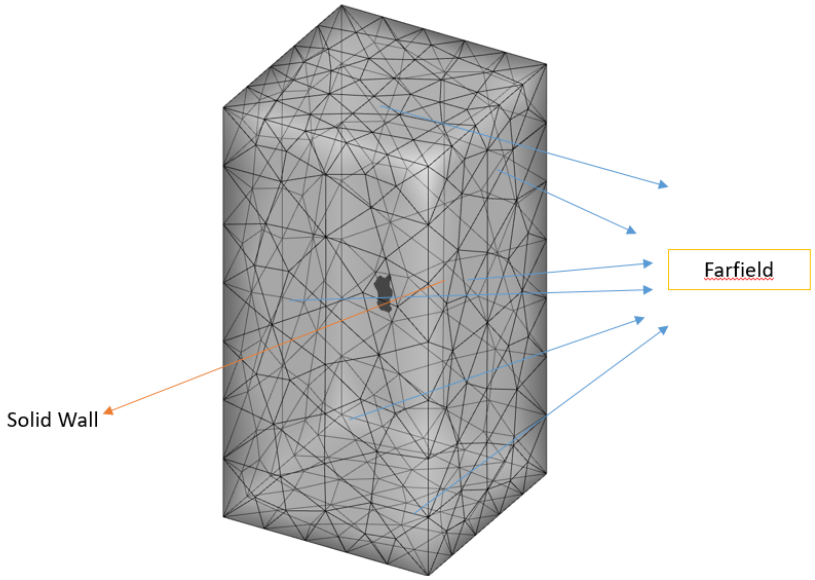

Figure 2.4 The fragment was modeled due to the far-field boundary condition

2.8 Flux Discretization

The Green-Gauss and JST (Jameson-Schmidt-Turkel) methods in flow solutions using the SU2 software were compared in this study. The Green-Gauss method provided more accurate interpolations on surfaces, while the JST scheme was favored for improved shock capturing. It enhances the accuracy of the outcomes that have been achieved and examines foreign particles in more detail.

CHAPTER 3

RESULTS

3.1 Mesh Independence Study

The mesh in this study is a hybrid-type grid containing tetrahedral and prismatic elements that were created. The boundary layer is filled with hexahedral elements of the size prismatic in the boundary layer to satisfy y+ $\approx$ 1 and resolve the viscous sublayer without wall functions. Prism cells and far-field boundaries tetrahedral cells are used for the rest of the domain. The thickness of the first cell along either side adjacent to the fragment surface was adjusted with great care as both sides had a near y+ value of 30 for all mesh configurations to sustain boundary layer resolution. As a result, with 1.2 growth on the cells following layer. It has a madden total of up to 47 layers in between boundaries which resulted in capturing near-wall flow behavior properly. In this study, the grid resolution used for computational analysis was determined carefully by making a full mesh-independent test with 4 different resolutions as shown correctly in Table 3.1. The final mesh layout included 1.5 million cells to capture the full details of the computational domain, but this mesh was computationally expensive for every case; therefore a coarse mesh of 200.000 cells provided lower resolution but also much less cost. The quality and solution of mesh directly impact on accuracy and reliability of results in simultaneous simulations. A too coarse mesh cannot capture important flow phenomena and a much too fine one means prohibitive computational costs. A lot of effort went into designing a suitable refining mesh for specific critical regions where phenomena like boundary layer transition or flow separation were expected, such as near the sharp edges and close to the surface of the fragment. The mesh independence studies were also carried out to ensure the selected resolution of the coarsest grid did not affect results adversely. A series of preliminary analyses were performed to thoroughly assess the effectiveness of each mesh size, with a 500.000 cell being deemed as providing an adequate balance between computational efficiency and accuracy. Since this mesh was fine enough to resolve the large-scale flow structures it is a recommended choice for CFD analysis. Finally, Mesh #2 with 500.000 cells was loaded in the SU2 CFD solver to perform detailed aerodynamic analyses of fragment

particles under different free stream flows as shown in Figure 3.1.

	Number of Cells	Drag Coefficient
1	0.177×10^6	1.34
2	0.5×10^6	1.39
3	1×10^6	1.41
4	1.5×10^6	1.41

Table 3.1 Drag coefficient for different cell counts

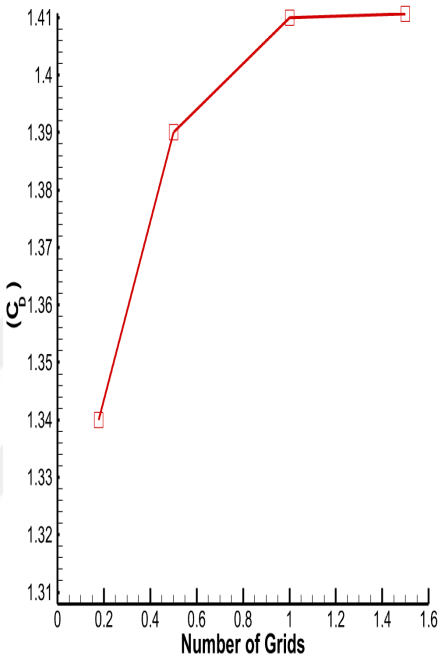

Figure 3.1 C_D at 0.8 Mach for different numbers of grid points

3.2 Orientation Angle

Latin Hypercube Sampling (LHS) is a method used for sampling from an N-dimensional distribution that is used in combination with some statistical techniques. This ensures a more uniform and efficient exploration of the input space, as opposed to plain random sampling. LHS divides the range of each input parameter into equiprobable intervals and selects one random value from each interval. While typical random sampling techniques would randomly select one value from the uniform interval, in LHS a new sample is taken to ensure that each parameter also only gives out values at these chosen points. This reduces the number of samples needed to achieve the same level of accuracy. Thus LHS was used to determine 30 different angles. The advantage of LHS

was that it was able to analyze the fragment from different angles as a result of the numbers it determined irregularly. LHS was used to rotate the fragment on the x-y-z principle axis. Thus, the fragment analyses different angles between 0° and 300°. θx° , θy°, θz° is angle that orientation about x-y-z principle axis. These angles are depicted in Table 3.2.

Table 3.2 The fragment orientation angle about x-y-z axis

Case	$\theta_{\mathbf{x}}^{\circ}$	$\theta_{\mathbf{y}}^{\circ}$	$\theta_{\mathbf{z}}^{\circ}$
1	0.84	283.53	244.56
2	180	273.21	123.54
3	275.37	253.65	24.57
4	235.77	70.56	72.78
5	45.39	177.92	34.77
6	112.29	2.91	80.07
7	156.78	137.64	137.82
8	282.15	88.8	168.93
9	35.28	53.94	148.89
10	269.64	65.49	279.36
11	228.24	125.4	155.94
12	122.79	33.39	285.51
13	55.26	182.31	186.33
14	148.47	146.49	292.35
15	166.59	223.38	53.73
16	23.94	235.83	222.27
17	208.08	201.57	90.66
18	62.61	11.67	200.28
19	137.58	27.45	238.08
20	180.84	93.87	18.61
21	77.31	154.17	63.03
22	92.34	214.59	49.05
23	218.11	111.3	194.76
24	87.12	267.36	264.69
25	259.08	246.81	101.4
26	294.24	298.80	255.15
27	243.18	160.59	216.06
28	104.52	103.53	3.32
29	195.75	45.21	172.59
30	13.56	193.62	114.81

3.3 Computed Flow Fields

The fragment as shown in was rotated at the angles in Table 3.2 and analysed using the $SU2$ program's Mach numbers of 0.8, 1.0, and 1.2. The average geometry obtained by averaging 30 different orientation views is shown in Figure 3.2.

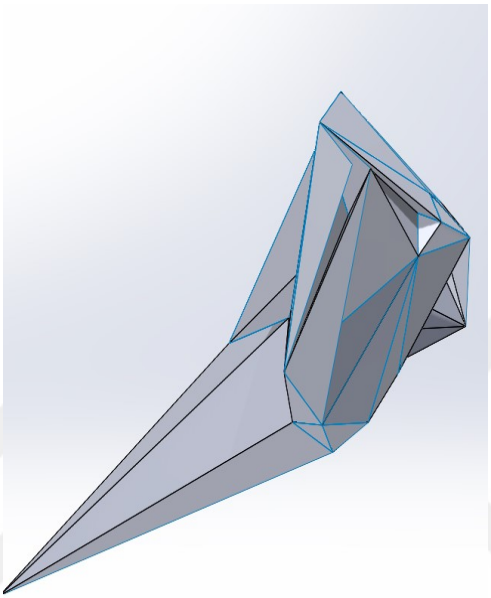

Figure 3.2 Average Shape

Table 3.3 presents the results of an aerodynamic analysis for a fragment rotated at a Mach number of 0.8. These findings illustrate the variability in the drag coefficient (C_D) and drag force across different exposed surface areas, highlighting how shape and orientation significantly impact the aerodynamic performance of non-spherical fragments. The study has shown that predicting such fragments' motion and drag characteristics can be complex, especially when they undergo random tumbling. Surrogate models have become essential for accurately estimating non-spherical fragments' drag coefficient (C_D), particularly when traditional empirical methods or comprehensive experimental data are insufficient or costly. A larger exposed area generally has a higher drag coefficient (C_D). However, this relationship is not completely linear. The average 0.96 of these C_D values were obtained from all analyses in the computations. When the C_D value is computed by taking the average geometry of 30 fragments, C_D the value is 0·94. While the average drag force of 30 cases is 40.20 N, the drag force of the average shape is 25.11 N. When the fragment

was analysed without being rotated at any angle, the C_D value was 1.39 and the drag force was 99.01 N. The exposed areas ranged from 211 mm^2 to 1634 mm^2. The smallest area is seen in Case 24 (211 mm^2). The average exposed area is 855.64 mm^2. The average drag force of these fragments is 40.20N. The mean C_D value at 0.8 Mach is obtained by considering the average drag force and the average exposed area as 1.02. The observed range of C_D in the study, spanning from 0.48 to 1.86, reflects substantial variability. This is consistent with existing studies demonstrating that C_D varies significantly depending on orientation and surface exposure relative to the flow. The analysis could further contribute to the current body of knowledge by emphasizing the shape-dependent behaviour of C_D and the resulting aerodynamic forces at specific Mach numbers.

These results could also enhance the understanding and modelling of fragment motion following an explosion, supporting the development of predictive models and safety protocols, as indicated in relevant research on the topic.

Table 3.3 Analysis result of the fragment obtained by rotating at Mach number of 0.8

Case	Exposed Area (mm^2)	C_D	DRAG(N)
1	581.00	1.70	44.78
2	461.00	0.75	15.68
3	812.19	0.76	27.99
4	412.00	0.58	10.84
5	1515.00	1.46	100.30
6	566.36	0.54	13.87
7	1145.55	0.91	47.27
8	464.88	1.00	21.09
9	1198.21	1.86	101.05
10	326.00	0.53	7.83
11	1285.94	0.91	53.06
12	480.10	0.65	14.15
13	1634.00	1.36	100.76
14	873.00	0.84	33.25
15	1040.00	0.84	39.61
16	1071.00	0.88	42.73
17	440.00	0.88	17.56
18	1578.00	1.29	92.30
19	1136.65	0.97	49.99
20	352.63	0.62	9.91
21	889.00	0.73	29.42
22	1108.00	0.94	47.22
23	839.00	0.70	26.63
24	211.00	0.86	8.23
25	341.50	1.34	20.75
26	447.60	0.48	9.74
27	1391.70	1.14	71.94
28	807.75	0.81	29.67
29	1347.00	1.21	73.90
30	913.05	1.08	44.71
Average	855.64	0.96	44.71
		1.02	
Average Shape	595.56	0.93	25.11

Table 3.4 shows some results of the aerodynamic analysis of a fragment tumbled at Mach number 1.0 and shows how exposed areas and orientations of a fragment vary with drag coefficient and drag force. Thus, C_D varies from 0.12 to 2.37 and this large range is indicative of a great range of aerodynamic behaviour depending on the orientation of the fragment during tumbling. At supersonic speeds, shock waves are formed, and these waves cause sudden changes in the pressure, temperature, and density of the fluid. These shock waves can cause the airflow to separate from the surface and increase the drag coefficient. The interaction between the shock waves and the boundary layer can increase the drag coefficient at supersonic speeds. The separation of the boundary layer from the flow can increase the pressure drag and lead to higher C_D values. High C_D values may indicate situations where such interactions are severe. The geometry of the fragment has a large effect on C_D at supersonic conditions. Sharp edges or abruptly changing surface slopes can cause shock waves to be stronger and therefore result in a higher drag coefficient. High C_D values can be an indication of the effects of such geometric features at supersonic conditions. The average $C_D$value was calculated as 1.21. The C_D value of the average shape is 1.11. The drag force of the average shape is 46.81 N. When the average drag force of the cases is calculated at 1 Mach, it is found to be 68.16 N. The average exposed area is 855.64 mm^2. The mean C_D value at 1.0 Mach is obtained by considering the average drag force and the average exposed area as 1.05. When the flow was analysed by exposing the fragment to an area of 1591 mm^2, the drag coefficient value was 1.71 and the drag force was 189.08 N. These results are in good agreement with the literature showing that non-spherical fragments undergo strong variability in their drag characteristics due to random tumbling since areas presented in each orientation against the flow are different, a factor directly influencing both C_D and drag forces experienced. As shown in this table, cases with greater areas tend to develop higher magnitudes of drag force; however, C_D values can vary independently due to the complex interactions between shape and flow alignment.

This analysis underlines the importance of the most advanced predictive models, such as surrogate models which are capable of making accurate estimations of C_D in real-time, especially for fragments in unpredictable tumbling scenarios. The models have shown promise toward complex aerodynamic response representation across vastly changing

orientations and Mach regimes, which are rather difficult to predict through traditional empirical methods alone.

Table 3.4 Analysis results of the fragment obtained by rotating at a Mach number of 1.0

Case	Exposed Area (mm^2)	C_D	DRAG(N)
1	581.00	2.37	97.66
2	461.00	1.04	33.84
3	812.19	0.71	40.79
4	412.00	1.780	51.93
5	1515.00	0.68	72.93
6	566.36	1.13	45.46
7	1145.55	1.35	109.62
8	464.88	2.28	74.90
9	1198.21	0.61	52.16
10	326.00	1.28	29.60
11	1285.94	1.10	99.73
12	480.10	1.65	56.23
13	1634.00	1.05	120.92
14	873.00	1.10	67.84
15	1040.00	0.12	9.01
16	1071.00	1.24	94.03
17	440.00	1.50	46.70
18	1578.00	1.24	138.90
19	1136.65	0.76	61.00
20	352.63	0.88	22.04
21	889.00	1.12	70.43
22	1108.00	0.88	69.36
23	839.00	1.08	64.12
24	211.00	1.84	27.42
25	341.50	0.62	14.94
26	447.60	1.33	42.28
27	1391.70	1.18	116.34
28	807.75	1.21	69.19
29	1347.00	1.42	135.03
30	913.05	1.71	110.30
Average	855.64	1.21	68.16
		1.05	
Average Shape	595.56	1.11	46.81

Table 3.5 shows the exposed area and corresponding drag coefficient (C_D) values of a fragment at a Mach number of 1.2 in 30 different cases. The aerodynamic analysis of the fragment at Mach 1.2 with data from 30 different orientations shows considerable variability in drag coefficient, C_D, and drag forces encountered. The value of C_D lies within the wide limit, starting from 0.69 in Case 26 to 2.35 in Case 9. This variation shows the variability of orientations on the aerodynamic forces that will act on the fragment. That would also agree with the various studies involving irregularly shaped fragments, in which it was observed that drag forces change owing to changes in both the amount of surface area exposed and its orientation relative to airflow. The average value of C_D for all configurations is 1.28, while the average drag force is 160.44 N. In contrast, the average shape of the C_D value is 1.23.

With an average exposure area of 855.64 mm^2 and an average drag force of 160.44 N, it becomes clear that a single drag coefficient may not capture the complexity for all orientations, but it gives very close results with the drag force of the average shape. The C_D value corresponding to the average expose area and average drag force is 1.35. Case 1 (C_D = 2.34, Exposed Area = 581 mm^2) and Case 9 (C_D = 2.35, Exposed Area = 1198.21 mm^2) have the highest drag coefficients. These high values indicate that these shapes encounter the most aerodynamic drag at Mach 1.2. Such high C_D values can often result from effects such as shock waves and boundary layer separation at supersonic speeds.

Table 3.5 Analysis results of the fragment obtained by rotating at a Mach number of 1.2

Case	Exposed Area(mm^2)	C_D	Drag(N)
1	581.00	2.34	138.78
2	913.00	1.25	116.35
3	812.19	1.07	88.71
4	412.00	0.82	34.33
5	1515.00	1.85	285.70
6	566.36	0.75	43.212
7	1145.55	1.21	141.87
8	464.88	1.32	62.60
9	1198.21	2.35	287.54
10	326.00	0.74	24.50
11	1285.94	1.27	166.86
12	480.10	1.10	53.62
13	1634.00	1.70	282.76
14	873.00	1.04	92.46
15	1040.00	1.18	124.93
16	1071.00	1.24	1360.829
17	440.00	1.21	54.41
18	1578	1.55	248.60
19	1136.65	1.27	147.70
20	352.63	0.89	31.90
21	889.00	0.89	80.23
22	1108.00	1.16	130.81
23	839.00	0.93	79.89
24	211.00	1.26	27.18
25	341.50	1.88	65.34
26	447.60	0.69	31.55
27	1391.70	1.38	196.46
28	807.75	1.18	97.23
29	1347.00	1.32	181.55
30	913.05	1.46	135.54
Average	855.64	1.27	160.44
		1.80	
Average Shape	595.56	1.23	74.68

The fragment was analysed to provide exposure to the flow without being rotated at any angle, as seen in Figure 2.3. Accordingly, Mach field results for Mach numbers 0.8, 1.0, and 1.2 are given in Figure 3.3. The drag coefficients of the CFD computed for the fragment without any orientation were 1.39, 1.71, and 1.76 at the Mach numbers of 0.8, 1.0, and 1.2. In Figure 3.4, low-velocity regions (blue and light blue regions) are observed upstream of the fragment, and high-velocity regions (green and yellow regions) are observed behind it. The flow velocity increases around the fragment and reaches higher values, especially behind it. This indicates that the flow accelerates as it passes around the fragment, and therefore the frictional resistance increases. Expansion shock waves occur when the flow accelerates and the pressure decreases. These waves occur when the flow expands and are usually formed downstream of the fragment in supersonic flow. In Figure 3.3, expansion waves can be observed, especially at the rear of the fragment. In the Mach flow field, areas where the speed increases and the pressure decreases at the rear of the fragment are observed, indicating the presence of expansion waves. There is no observation regarding oblique or bow shock waves. It can be seen when analysed at higher Mach numbers. Figure 3.4 depicts non-dimensional pressure fields around the fragment for the maximum exposed area to the flow field. A high-pressure region (red and orange regions) is formed at the front of the fragment, indicating that the flow impinges on the front surface of the fragment and accumulates there, as seen in Figure 3.4. The pressure drops rapidly at the back of the fragment (blue and green regions). This indicates that a large pressure force is generated at the front of the fragment, creating a low-pressure area at the downstream of the fragment. While high pressure generally occurs upstream of the fragment, low pressure occurs downstream of it. This situation shows the friction resistance and the forces resulting from the pressure difference that the fragment encounters while moving in the flow. It can be said that as the flow rate increases, the pressure difference becomes more pronounced and this significantly affects the aerodynamic properties of the fragment. Pressure drag is the drag force resulting from pressure differences exerted on the surface of a fragment. This type of drag becomes particularly significant at supersonic and hypersonic speeds. A fragment has high pressure at the front and low pressure at the rear; this pressure difference creates a drag force towards the rear of the fragment. This drag is a significant component of the total drag force. This pressure difference

around the fragment is the main source of pressure drag. High pressure at the front of the fragment pushes it back in the direction of flow, while low pressure at the back increases this force. This pressure difference creates significant resistance on the fragment, which is called pressure drag. This pressure difference is observed in the images. In particular, the pressure contours show a typical pressure drag situation characterized by high pressure in the front of the fragment and low pressure in the back. This situation varies depending on the aerodynamic structure of the object and the flow conditions.

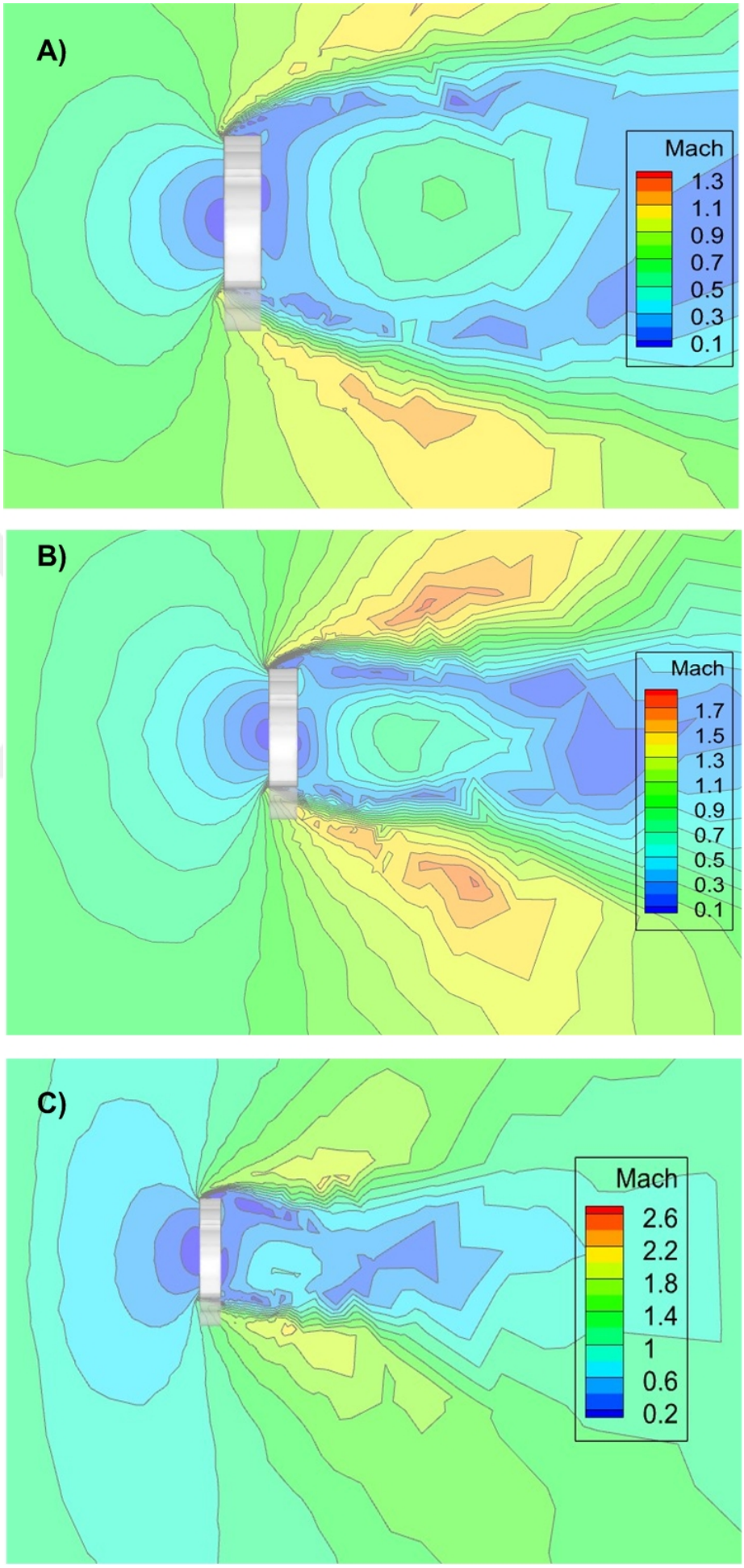

Figure 3.3 Ma number field of the fragment of A) M=0.8, B) M=1.0, and C) M=1.2

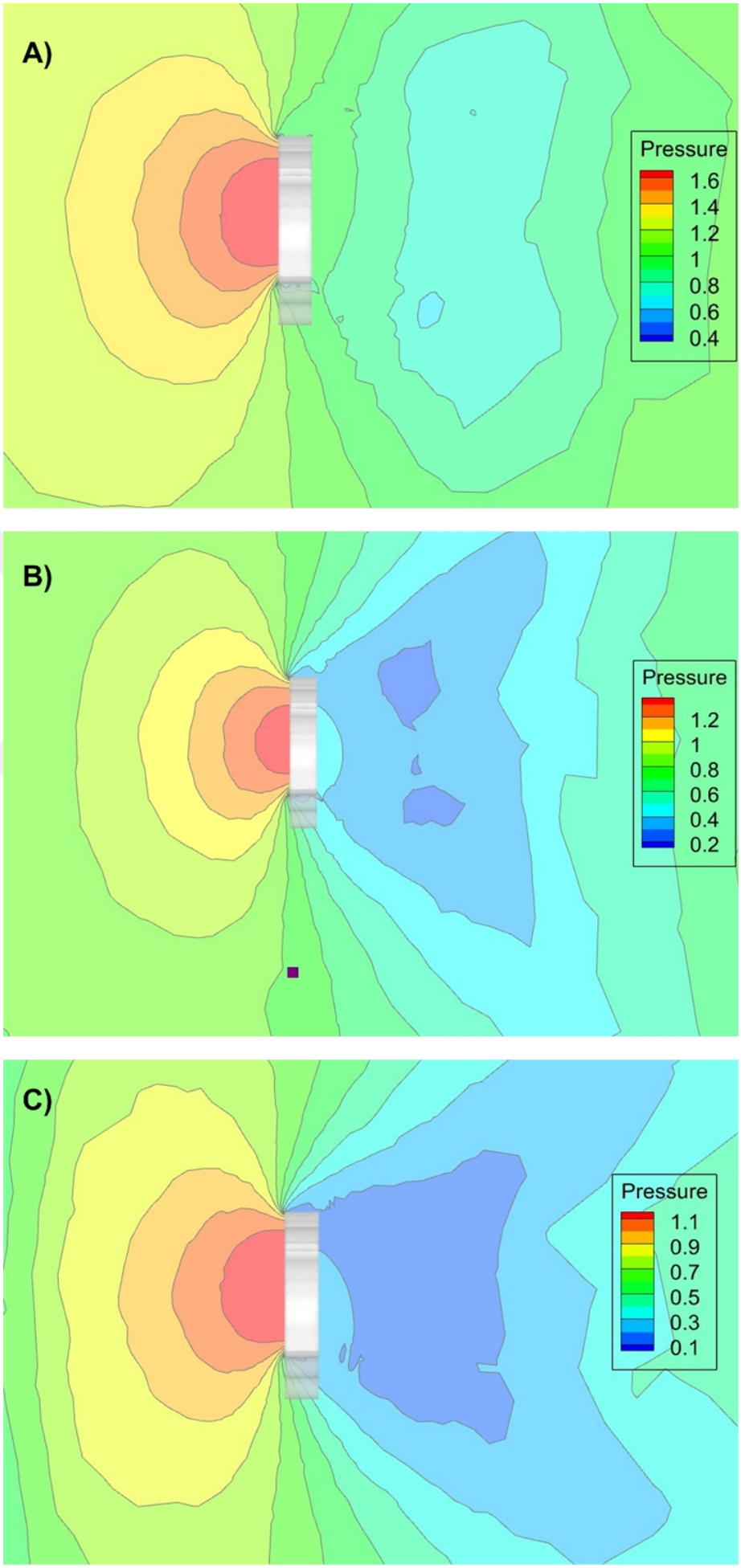

Figure 3.4 Nondimensional pressure field of the fragment of A) M=0.8, B) M=1.0, and C) M=1.2

3.4 Conclusion

This thesis investigated the aerodynamic properties of a non-spherical fragment at Mach numbers of 0.8, 1.0, and 1.2 over 30 different orientations, focusing on the drag coefficient C_D, drag force, and exposed area for each case considered. The goal is to calculate three main values of C_D: the average of C_D over all orientations, the C_D deduced from the average drag force and exposed area, and C_D of the average geometry. Results indicated large variability C_D depending on orientations; C_D is found to range over wide limits depending on Mach numbers. For instance, the variation range of C_D at Mach 0.8 was quite large, following similar trends as recorded at Mach 1.0 and 1.2, where C_D values would go from 0.69 to 2.35 at the highest setting in this paper. This supports the evidence in the literature, which explains that these changes are due to variations in shape, exposed area, and individual fragment orientations to the flow, particularly non-spherical fragments [46].

The computed average values of C_D for the same Mach numbers amount to 1.08, 1.21, and 1.27 for Mach 0.8, 1.0, and 1.2, respectively, leading to increased average drag forces with increasing Mach numbers. Thus, it can be concluded that the average shape exhibits consistently lower C_D values, resulting in reduced drag forces across all tested Mach conditions. The average of C_D at Mach 0.8 had an average value of 1.02. The corresponding average drag force stays approximately at 40.20 N. Merely the C_D value from the average geometry was 0.93, hence leading to a lower drag force of 25.11 N. Whereas the average at Mach 1.0 was 1.21, corresponding to 68.16 N of drag force, for the average geometry it came down to 1.11, which corresponded to 46.80 N. For Mach 1.2, this average C_D was increased to 1.27, with its corresponding drag force being 160.44 N, while for the average geometry, the C_D was 1.23 with its corresponding drag force of 74.68 N. While larger exposed areas generally corresponded to higher C_D values across the Mach ranges, the relationship was, in fact, not strictly linear. Comparing these results, the average C_D across all orientations provides the general trend in the aerodynamic behaviour. This reduction outlines the great potential for using optimized geometries in trajectory calculations, since computational simplicity and efficiency play a very important role there. However, the variation of C_D values over

different orientations underlines the issue of considering orientation-specific effects in safety-critical applications. In other words, this test shows that the C_D provided by the average geometry is a computationally efficient and valid choice for trajectory predictions in general and in scenarios where reduced computational complexity is acceptable. Where highly accurate modelling is required, variability accounting by advanced surrogate models or orientation-specific analyses is preferred. One will greatly balance the accuracy and efficiency concerns in aerodynamics modelling with both methods for non-spherical fragments over supersonic regimes.

The cases that had virtually identical exposed areas at each Mach setting often exhibited variant C_D values, which demonstrated how fragment geometry and orientation can influence drag behaviour. The use of an average C_D in trajectory calculations is, computationally, several orders of magnitude more convenient, particularly in real-time applications. The average value of C_D does not represent the actual values developed during tumbling motions at various orientations; however, it provides a reasonable compromise between accuracy and computational simplicity. Studies confirm that, among these, models with average values of C_D, such as 2-DOF and 3-DOF models, give reliable predictions with less computational cost, useful in situations where the speed and repeatability of results are to be emphasized.

In conclusion, while it is appropriate to use average shape and average C_D values for 0.8 and 1.0 Mach, 1.2 Mach may not give accurate results. Although enhanced models such as 6-DOF or even machine learning-based surrogates can provide accurate, orientation-dependent drag predictions, the averaging approach for C_D has been continuously successful, showing computational efficiency within a wide range of Mach numbers. Such balance will be of particular benefit in safety-critical applications because accurate, yet feasible predictions of the aerodynamic forces are crucial for real-time decisions and risk assessments. Addressing these issues in future studies might thus provide even more complete surrogate models, by combining both average and orientation-specific predictions of C_D in a manner that can supply adaptable solutions under an even larger range of conditions.

REFERENCES

[1] Barwey S., "Drag coefficient analysis of arbitrary fragment geometry with emphasis on meshing sensitivity studies." Sandia National Lab.(SNL-NM), Albuquerque, NM (United States), Tech. Rep., 2020.

[2] MCCLESKEY F. and BOARD E. S., "Drag coefficients for irregular," 1988.

[3] Cardona V. and Lago V., "Aerodynamic forces of interacting spheres representative of space debris re-entry: Experiments in a supersonic rarefied wind-tunnel," *Acta Astronautica*, 2022.

[4] Catovic A., Kljuno E., and Voloder A., "Analysis of flow around high speed irregularly shaped bodies using numerical simulations," *International Journal of Advanced and Applied Sciences*, 2018.

[5] Cheeseman I., "Fluid-dynamic drag: Practical information on aerodynamic drag and hydrodynamic resistance." *The Aeronautical Journal*, 1976.

[6] Xin D., Zeng J., and Xue K., "Surrogate drag model of non-spherical fragments based on artificial neural networks," *Powder Technology*, 2022.

[7] Anderson J., *EBOOK: Fundamentals of Aerodynamics (SI units)*. McGraw hill, 2011.

[8] White F. M. and Majdalani J., *Viscous fluid flow*. McGraw-Hill New York, 2006.

[9] Anderson J. D., "Modern compressible flow: with historical perspective," *(No Title)*, 1990.

[10] Kuethe A. M. and Chow C.-Y., *Foundations of aerodynamics: bases of aerodynamic design*. John Wiley & Sons, 1997.

[11] Pope A. and Goin K., *High-speed Wind Tunnel Testing*. R. E. Krieger Publishing Company, 1978.

[12] Liepmann H. W. and Roshko A., *Elements of gasdynamics*. Courier Corporation, 2001.

[13] Schlichting H. and Gersten K., *Boundary-layer theory*. springer, 2016.

[14] Sahu J., "Time-accurate numerical prediction of free-flight aerodynamics of a finned projectile," *Journal of Spacecraft and Rockets*, 2008.

[15] Gui Z., Wang X., and Li W., "Dynamic perception-based vehicle trajectory prediction using a memory-enhanced spatio-temporal graph network," *ISPRS International Journal of Geo-Information*, 2024.

[16] Lv Z., Li J., Dong C., Wang Y., Li H., and Xu Z., "Deepptp: A deep pedestrian trajectory prediction model for traffic intersection." *KSII Transactions on Internet & Information Systems*, vol. 15, no. 7, 2021.

[17] Wang J., Guo C., Guo M., and Chen J., "Jointly learning agent and lane information for multimodal trajectory prediction," *arXiv*, 2021.

[18] Xue H., Huynh D. Q., and Reynolds M., "Scene gated social graph: Pedestrian trajectory prediction based on dynamic social graphs and scene constraints," *arXiv*, 2020.

[19] Lin X., Zhang Y., Wang S., Piao X., and Yin B., "Multiagent trajectory prediction with global-local scene-enhanced social interaction graph network," *Computer Animation and Virtual Worlds*, vol. 35, no. 3, p. e2237, 2024.

[20] Yoon J. S., Li Z., and Park H. S., "3d semantic trajectory reconstruction from 3d pixel continuum," in *2018 IEEE/CVF Conference on Computer Vision and Pattern Recognition*, 2018.

[21] Zhao W., Wang D., Gao K., Wu J., and Cheng X., "Large-scale long-term prediction of ship ais tracks via linear networks with a look-back window decomposition scheme of time features," *Journal of Marine Science and Engineering*, 2023.

[22] Mark H. and Davis S., *Aerodynamics of Missiles and Projectiles*. American Institute of Aeronautics and Astronautics (AIAA), 1985.

[23] Heitsch F., Hartmann L. W., and Burkert A., "Fragmentation of shocked flows: gravity, turbulence, and cooling," *The Astrophysical Journal*, 2008.

[24] Padoan P. and Nordlund Å., "The stellar initial mass function from turbulent fragmentation," *The Astrophysical Journal*, 2002.

[25] Veysset D., Kooi S. E., aznev A., Tang S., Mijailovic A. S., Yang Y. J., Geiser K., Van Vliet K. J., Olsen B. D., and Nelson K. A., "High-velocity micro-particle impact on gelatin and synthetic hydrogel," *Journal of the mechanical behavior of biomedical materials*, 2018.

[26] Sureshkumar A. and Sridhar B., "Experimental studies on decay and spread characteristics of an overexpanded triangular supersonic jet," *Fluid Dynamics*, 2019.

[27] Babinsky H. and Harvey J. K., *Shock wave-boundary-layer interactions*. Cambridge University Press, 2011.

[28] Eddegdag N., Naamane A.-e., and Radouani M., "Investigation of viscous supersonic laminar flows around f-16 airfoil: experimental, numerical, and analytical approaches," *Physica Scripta*, 2023.

[29] Mateescu D., "Explicit exact and third-order-accurate pressure-deflection solutions for oblique shock and expansion waves," *The Open Aerospace Engineering Journal*, 2010.

[30] Catovic A. and Kljuno E., "Prediction of aerodynamic coefficients for irregularly shaped body using numerical simulations," *International Journal of Advanced and Applied Sciences*, 2018.

[31] Zecevic B., Terzic J., Catovic A., and Serdarevic-Kadic S., "Characterization of distribution parameters of fragment mass and number for conventional projectiles," in *Proceedings of the conference (assuming you know the conference name)*, April 13 2011.

[32] Ryabinin A. and Kuzmin A., "Transonic flow simulation in a bent channel using su2 software," in *2020 Ivannikov Ispras Open Conference (ISPRAS)*. IEEE, 2020.

[33] Venkatakrishnan V., "On the accuracy of limiters and convergence to steady state solutions," in *AIAA Aerospace Sciences Meeting and Exhibit*. Reno, NV: AIAA, January 1 1993.

[34] Rembaut N., Joussot R., and Lago V., "Aerodynamical behavior of spherical debris in the supersonic and rarefied wind tunnel marhy," *Journal of Space Safety Engineering*, 2020.

[35] Vashchenkov P., Kashkovsky A., and Ivanov M., "Aerodynamics of fragment in spacecraft wake," in *Rarefied Gas Dynamics*, 2003.

[36] Ambrosio A. and Wortman A., "Stagnation-point shock-detachment distance for flow around spheres and cylinders in air," *Journal of the Aerospace Sciences*, 1962.

[37] Billig F. S., "Shock-wave shapes around spherical-and cylindrical-nosed bodies." *Journal of Spacecraft and Rockets*, 1967.

[38] Tiumentsev A. Y. and Tiumentsev Y. V., "Motion control of supersonic passenger aircraft using machine learning methods," *Optical Memory and Neural Networks*, 2023.

[39] Kljuno E. and Catovic A., "Contribution to compressibility modelling in the estimation of forces acting on projectile fragments." *Advances in Military Technology*, 2020.

[40] Gerasimov S. I., Erofeev V. I., Kikeev V. A., Kuzmin V. A., Zharov A. N., and Novikov I. A., "Experimental and computational research of supersonic and hypersonic flow around cube shaped fragments in the air," in *IOP Conference Series: Materials Science and Engineering*. IOP Publishing, 2020.

[41] Dioguardi F. and Mele D., "A new shape dependent drag correlation formula for non-spherical rough particles. experiments and results," *Powder Technology*, 2015.

[42] Alatorre-Ibargüengoitia M. A. and Delgado-Granados H., "Experimental determination of drag coefficient for volcanic materials: calibration and

application of a model to popocatépetl volcano (mexico) ballistic projectiles," *Geophysical Research Letters*, 2006.

[43] Barri N., "Dynamics of two spherical objects in supersonic flow," in *Doklady Physics*. SP MAIK Nauka/Interperiodica Dordrecht, 2010.

[44] Li T., Sui J., Gong S., and Wu C., "Dynamical separation of rigid bodies in supersonic flow," *Science China Technological Sciences*, vol. 58, pp. 2110–2121, 2015.

[45] Spalart P. and Allmaras S., "A one-equation turbulence model for aerodynamic flows," in *30th aerospace sciences meeting and exhibit*, 1992.

[46] Nista L. and Saracoglu B. H., "Numerical investigation of the stratofly mr3 propulsive nozzle during supersonic to hypersonic transition," p. 3843, 2019.